Check for updates

Received: 12 July 2024 | Revised: 29 April 2025 | Accepted: 15 August 2025

DOI: 10.1002/suco.70315

ARTICLE

fib CEB-FIP WILEY

Time-domain analysis of signal morphology and features as suitable surrogates for structural monitoring

Kapil Nichani[1,2] | **Steffen Uhlig**[3] | **Victor San Martin**[1] | **Yogi Jaelani**[4] | **Kirstin Frost**[1] | **Carina Beering**[5] | **Karina Hettwer**[1] | **Sven Knoth**[5] | **Sylvia Keßler**[4]

[1]QuoData GmbH, Dresden, Germany

[2]Institute of Nutritional Sciences, University of Potsdam, Potsdam, Germany

[3]QuoData GmbH, Berlin, Germany

[4]Department of Engineering Materials and Building Preservation, School of Mechanical and Civil Engineering, Helmut Schmidt University Hamburg, Germany

[5]Department of Mathematics & Statistics, School of Economic and Social Sciences, Helmut Schmidt University Hamburg, Germany

Correspondence
Sylvia Keßler, Department of Engineering Materials and Building Preservation, School of Mechanical and Civil Engineering, Helmut Schmidt University Hamburg, Germany.
Email: sylvia.kessler@hsu-hh.de

Funding information
European Union - NextGenerationEU

Abstract

The holy grail of signal processing is getting suitable features that act as surrogates for damage conditions in structural monitoring. These features, which describe the characteristic shape and pattern of signals (i.e., their morphology), can be descriptive or predictive of the condition of the structure and help in the effective management of repairs and damage control. The signal measurement data and the features derived from them are highly affected by a myriad of on-ground conditions referred to as noise factors. In this study, we collect data from accelerometers using a factorial design in a laboratory setting with a shaker that are put under the effect of some noise factors that can potentially have a large influence on the sensor outcome. We gather a compendium of candidate time-domain signal features and quantitatively evaluate using the accelerometer data. Of the many possible noise factors, we vary cable length, vibration of cable, and electromagnetic interference and investigate the measurement dispersion effects on the signal features. We introduce and plot "normalized profiles" a methodology for extracting key morphological characteristics from periodic signals. We propose the calculation and use of simple S/N ratio metrics to evaluate the suitability of a feature and how robust they are to the noise factors. This study contributes to advancing SHM methodologies by expanding the range of tools available to civil engineers for assessing signal morphology and identifying suitable surrogates describing the condition of a structure.

KEYWORDS

factorial design of experiments, measurement uncertainty, signal features, structural health monitoring

This is an open access article under the terms of the Creative Commons Attribution License, which permits use, distribution and reproduction in any medium, provided the original work is properly cited.
© 2025 The Author(s). *Structural Concrete* published by John Wiley & Sons Ltd on behalf of International Federation for Structural Concrete.

1 | INTRODUCTION

Feature extraction, especially the study of a signal's shape and structure is considered the holy grail of signal processing across various engineering disciplines.[1] This importance extends to Structural Health Monitoring (SHM) as underscored by Axiom IV(a) of the Fundamental Axioms of SHM, which states, "Sensors cannot measure damage, feature extraction through signal processing and statistical classification are necessary to convert sensor data into damage information."[2] In other words, features that describe the shape, structure and morphology of the signal are used as surrogates to identify type of damage, assess extent of damage, investigate effect of operation or environmental parameters, among others. Having access to reliable feature cannot only serve well to address all levels of Rytter's hierarchy of SHM tasks (i.e., damage detection, localization, assessments and prognosis) but also with troubleshooting issues, which is of interest to structural engineers and operators (e.g., civic bodies), alike.[3]

Civil structures such as a bridges, which are of interest in the paper, can have monitoring systems generate large amounts of data, sometimes at a high sample frequency.[4,5] Without data processing or feature extraction, the continuous inflow of sensor data can increasingly become overwhelming for users, making it practically unusable, like "catching a waterfall in a cup". In face of ambiguity of future utility and being wary of missing potentially important signals, structural operators end up erring on the side of caution by saving all available data. Cawley describes an appalling anecdote in his review, in which multi-channel, high sampling rate, sensor data from a bridge was being saved due to indecision about which specific details to retain and which insightful features to extract for the bridge's analysis.[6] Notwithstanding the substantial cost deterrent of operating continuous monitoring in this manner,[7,8] identifying appropriate surrogate features from signal data can significantly streamline the practical application of monitoring systems, thereby accelerating their integration. Clearly, features are important not only for data mining and dimensionality reduction but also for information management.

Signal features can be derived in the frequency domain (e.g., eigenfrequencies, mode shapes, etc.),[9] which typically reflect changes in structure stiffness, or in the time domain (e.g., peaks, RMS, etc.), which generally capture time-localized patterns.[10] A substantial body of research has interrogated the merits and deficiencies of methodologies to obtain features and their applications to monitoring structures. Yet, a few key issues remain. First, a widespread challenge persists in obtaining (signal) data associated with the damaged state, resulting in a common bias toward features that may not accurately indicate damage. Here, well-curated benchmark studies with vibrational sensor data acquired from both damaged and healthy states help to alleviate some of the challenges.[11,12] Second, the challenge is the small signal-to-noise ratio (S/N ratio) of the features due to the effect of influencing factors experienced on the structure (e.g., sensor related variability, varying environmental or operational conditions, etc.) masking the effects of structural changes.[13,14] Several studies propose options to offset or correct for the effects of influencing factors. Buckley et al. recently conducted a comparison of features where they checked different supervised machine learning (ML) model performance based on the features it was trained on.[15] However, the question regarding how to assess if features are insensitive to influencing factors on the ground and how to identify and determine which features are suitable remains a challenge.[6] The focus of this work is to address this challenge.

There are many influencing factors that act as sources of variability contributing to the uncertainty of the SHM system. Given that sensors and measurement data play a pivotal role in SHM systems, "measurement uncertainty" (or MU) emerges as a significant type that warrants particular attention. The discourse on uncertainty typically distinguishes between epistemic and aleatoric types.[16] The reader should be careful not to confuse the uncertainty caused by variations in models or data processing with the uncertainty caused by variability on the bridge.[17,18] From a metrological perspective, the term MU is defined as a non-negative parameter that quantifies the spread of the values attributed to a measurand (in this case the feature of interrogation), based on the information utilized.[19] Uncertainty in the sensor data can arise due to (a) sampling or digitization errors depending on its quality and calibration,[20] (b) environmental and operational factors such as temperature, pressure, humidity, loading, etc., (c) human factors such as the installation process, and (d) sensor-related factors such as cables connecting the sensors to data acquisition systems (DAQs), electromagnetic interference from cell towers, among others.[21,22] The uncertainty outlined in the sensor specification document by the manufacturer may serve as a reasonable estimate for (a). However, it is an inadequate measure under additional considerations outlined in (b), (c), and (d), for which the value is likely to be too low.

To this end, we have a twofold aim: (a) how do different features that describe the shape and morphology of a sensor signal vary under the effect of sources of variability, and (b) how to identify which one of these surrogate features is suitable, by determining the MU. With these aims, we utilize the shaker experimental data collected

17517648, 0, Downloaded from https://onlinelibrary.wiley.com/doi/10.1002/suco.70315 by Universitätsbibliothek, Wiley Online Library on [09/09/2025]. See the Terms and Conditions (https://onlinelibrary.wiley.com/terms-and-conditions) on Wiley Online Library for rules of use; OA articles are governed by the applicable Creative Commons License

using a factorial design to systematically study different features under the influence of three chosen noise factors—electromagnetic interference (EMI), length of cable, and vibration of cable. In this paper, we use the term 'signal morphology' to refer to the characteristic shape, structure, and pattern of time-domain signals, including their geometric features, temporal characteristics, and distinctive waveform attributes. While morphology analysis is well established in biomedical signal processing,[23] where it describes the characteristic shapes of physiological waveforms, its application in SHM extends this concept to vibration signatures. Signal morphology in our context encompasses both qualitative aspects (visual patterns) and quantitative features (statistical descriptors) that characterize the time-domain representation of structural responses. These morphological characteristics serve as potential indicators of structural conditions, similar to how ECG morphology indicates cardiac health. We further assess the data in the time domain. We propose a procedure to extract "normalized profiles" which provides a signature of the entire signal trace to study the shape and morphology. Further, we list time-domain features that can be surrogates for signal shape and morphology. We evaluate these features using the experimental data and describe the uncertainty in measurements. These features are then compared for different design and noise factors. We propose and evaluate the S/N ratio as a performance measure to efficiently find suitable features for bridge monitoring. To the authors' knowledge, no other groups have reported the use of such an experimental design to acquire sensor data and use it to characterize the expected dispersion in the feature values and derive an S/N ratio from it.

2 | METHODS

2.1 | Experimental design

A factorial design (FD) based on the concepts as described in ISO TS 23471[24] was developed for the purposes of studying the sensor outcomes under the effect of sources of variability simulated in laboratory experimental conditions and determining MU.[22] The FD allows for the simultaneous exploration of various factors, systematically altered across multiple levels.[25] Factors and factor levels in a factorial design are selected based on the typical variation seen under routine conditions. A factor can be one of two types—design or noise factor.[26] For the FD study, these factors were varied, and the sensor responses were studied. To mimic the conditions of SHM on a bridge, a shaker table apparatus was set up (detailed description in the following section).

Design factor are those that have a direct influence on the system. In the present context, they pertain to the dynamics of the shaker that change the oscillation pattern in a defined way—specifically the shaker's acceleration and frequency. The latter is varied at two levels, that is, 5 and 25 Hz, and the former is varied at three levels, that is, 1, 3 and 5 m/s^2. Thus, resulting in $3 \times 2 = 6$ design factor combinations (hereafter referred to as cases).

Noise factors are those that are hard to control during a real-life scenario or their usage is often deemed impractical or cost prohibitive.[26] However, in experimental settings, it is feasible to establish fixed levels for the noise factors and systematically change them in conjunction with design factors. Noise factors that were chosen for this study include length of cables, vibration frequency of cable, and EMI. Details of the factor levels can be found in Table 1.

In our recent work, we identified and summarized different sources of variation in an Ishikawa diagram.[22] From this Ishikawa diagram, we selected three important sources of variability that affect the sensor outcome. The selection of these factors is driven by practical issues encountered in bridge monitoring systems. For instance, the length of the cable is crucial as the wiring configuration significantly influences the sensing performance. This is due to the distance between sensors and DAQs, looping, and the grounding of the cable.[12,27,28] Furthermore, vehicular or train traffic and loading on a bridge can cause cable vibrations, which could potentially introduce measurement errors.[28,29] Lastly, EMI is taken into account because the proximity of cell-phone towers, electrical power lines, and other sources of EMI can distort measurements or cause malfunctions in the sensing system.[27,30] The factorial design using the above chosen factors was used to ensure identical noise scenarios for all considered conditions of frequency and acceleration.

The cable connecting sensor to the data acquisition system was elongated in increments of 25 m, starting from 25 m and going up to 100 m. Additionally, this cable was also vibrated. Cable vibration was varied at three levels, 0, 15 and 25 Hz. Two levels of EMI were defined: the absence of additional electromagnetic disturbance other than the background effect, and the application of sources of EMI in the surrounding area. For each of the six cases, there were $4 \times 3 \times 2 = 24$ possible configurations, hereafter referred as settings.

2.2 | Laboratory setup

The experimental setup is illustrated in Figure 1. The experiment utilized two triaxial acceleration sensors[27]

17517648, 0, Downloaded from https://onlinelibrary.wiley.com/doi/10.1002/suco.70315 by Universitätsbibliothek, Wiley Online Library on [09/09/2025]. See the Terms and Conditions (https://onlinelibrary.wiley.com/terms-and-conditions) on Wiley Online Library for rules of use; OA articles are governed by the applicable Creative Commons License

TABLE 1 Description of design and noise factors along with factor levels chosen for the experimental design.

Type	Name	Unit	Factor levels
Design factors	Acceleration (Shaker)	m/s^2	1, 3, 5
	Frequency (Shaker)	Hz	5, 25
Noise factors	Length of cable	m	L0 = 25, L1 = 50, L2 = 75, L3 = 100
	Vibration frequency of cable	Hz	F0 = 0, F1 = 15, F2 = 25
	Electromagnetic interference	$\mu W/cm^2$	EMI0 ≈ 0.01, EMI1 ≈ 26

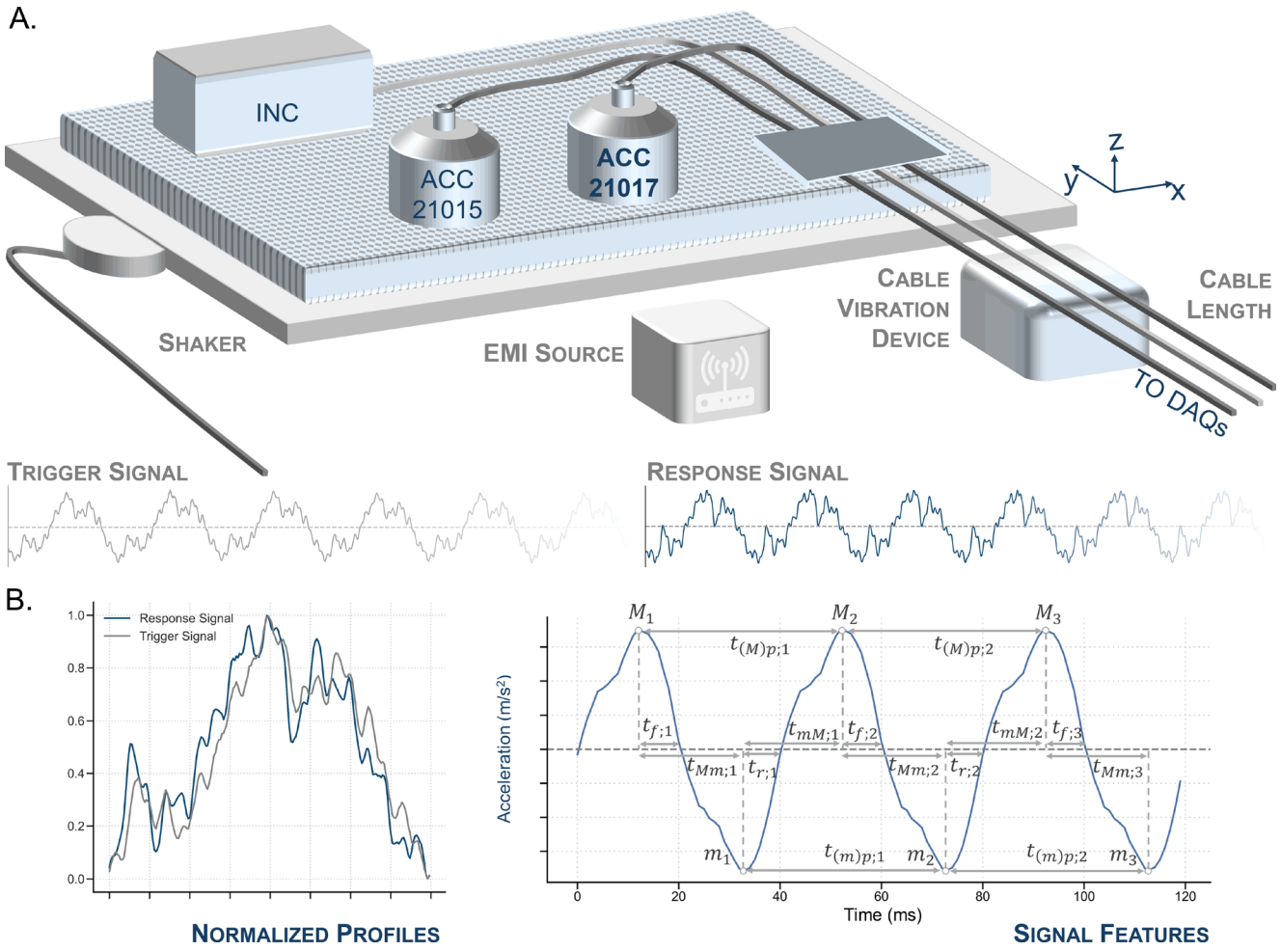

FIGURE 1 Illustration of the experimental setup and schema of analyses. (a) Schematic showing the shaker table apparatus, sensors, and noise factors. The shaker has three mounted sensors—one inclinometer (INC) and two accelerometers (ACC 21015 and ACC 21017). Cable length connecting the sensors and the DAQs was extended. Cables were vibrated using a vibration device. The WLAN box was placed in the vicinity as an EMI source. (b) Analyses performed in the study showing normalized profiles and a selection of signal features.

and one inclination sensor mounted magnetically atop a shaker. Accelerometer data was acquired at a sampling frequency of 1 kHz, while inclinometer data was recorded at 100 Hz. The specifics of the experimental configuration are likewise outlined in a concurrently reported study.[22]

An APS 420 ELECTRO-SEIS shaker was utilized, which generated the forcing signal that was then recorded by the sensors. Alongside the response signal, the trigger signal directly originated from the shaker amplifier and was also recorded. This signal serves as a proxy for the actual dynamics of the shaker. This shaker is a long-stroke electrodynamic force generator that can be operated independently or in conjunction with auxiliary table kits, which provide horizontal motion for components or model structures affixed to the table. The

17517648, 0, Downloaded from https://onlinelibrary.wiley.com/doi/10.1002/suco.70315 by Universitatsbibliothek, Wiley Online Library on [09/09/2025]. See the Terms and Conditions (https://onlinelibrary.wiley.com/terms-and-conditions) on Wiley Online Library for rules of use; OA articles are governed by the applicable Creative Commons License

shaker was set to operate in its horizontal vibrational mode. It was configured to generate sine waves with frequencies and amplitudes defined according to the design factors of the experimental settings.

Design factors were used to establish the working frequency and acceleration parameters of the shaker for each setting. Concerning noise factors, different cable lengths were achieved by connecting successive extension cables to the sensors. Cable vibration was induced by mounting them on a shaking table, which imparted constant-frequency vibration. EMI was induced using WLAN boxes placed in the vicinity of the shaker area.

The factorial design resulted in 144 combinations of design and noise factors (see Table S1) for which data acquisition was performed for a total period of 15 min each. Table S2 shows the available channels recorded.

2.3 | Signal data analyses

The signal processing analyses can be broken down into three main parts. First, the changes in signal shape and morphology were investigated under different conditions (changing noise factors). Next, 19 features based on the raw trace were evaluated for various signal lengths, from one oscillation to the complete 15-min series. Additionally, 4 features based on normalized profiles were assessed. Lastly, uncertainty quantification was done based on the above features to study the variation of the signal features under the influence of the noise factors and S/N ratios were calculated.

2.3.1 | Normalized profiles

The overall goal of the following steps is to achieve repeating segments with pronounced patterns, which are normalized in order to allow comparison of these profiles for a given factor level and between factor levels. Note that accelerometer data is often utilized to identify interesting frequencies. We start with estimating the dominant wavelength. Taking the argmax of the power spectrum density (psd) is a common approach. In contrast, we calculate here a robust variogram, that is, the "madogram" proposed in Cooley et al.,[31] namely

$$\nu(h) = \frac{1}{2} E\,|X_{i+h} - X_i\,| \qquad (1)$$

for a data series $\{X_i\}_{i=1,2,\ldots,n}$ and lag $h \in \{1, 2, \ldots, H\}$. For a fixed h, we replace $\nu(h)$ by an estimate (just the sample average counterpart). Then h which minimizes the estimate $\widehat{\nu}(h)$ is taken as principal wavelength λ_p. Because the nominal shaker frequencies, that is, 5 or 25 Hz, are quite dominant, we found for a sampling frequency of 1 kHz with both methods (madogram and psd) the principal wavelength $\lambda_p = 200$ and $\lambda_p = 40$ milliseconds (ms), respectively. Thus, the interesting segments are either 200 or 40 data points long. In the sequel, we quote λ_p with and without its unit depending on the context. Note that the output is just one oscillation. With oscillation we denote a subset of $\{X_i\}$ that has the same length as the primary wavelength.

For each factor level, we collected 15 min long series. We pick from each minute the first 10 s, and obtain the aforementioned segments from which a smooth profile for each minute was derived by calculating point-wise medians. As a result, we obtain 15 representative profiles per setting, that is, one combination of the considered factor levels. Eventually, all profiles are normalized by subtracting the profile minimum and dividing by the profile range. These normalized profiles reside in the interval $[0, 1]$. The procedure was followed for both the trigger signal and the accelerometer response signal.

2.3.2 | Signal features

In our discourse, we define a "signal feature" as any quantifiable parameter extracted from a signal. There exists a multitude of signal features or characteristics that can describe the signals collected from vibration sensors. We identified 23 time-domain features reported in the literature, not only in the field of SHM but also generally in digital signal processing. Some of these features have been borrowed from other application areas, such as biological signal processing, which also includes sensing.

The definition and descriptions of these features are summarized in Table 2. This table includes the feature symbol and a mathematical definition. Let $\{x_i\}_{i=1,\ldots,n}$ be the analyzed segment with $\overline{x}$ denoting the average of these x_i. Within the series we find n_c cycles having the principal wavelength, for instance $n_c = 10\,\text{s}/200\,\text{ms} = 50$ for 5 Hz. Nineteen features were derived from the accelerometer signals without any preprocessing. To compare the feature variability at short and long time windows, features were derived by investigating five different time windows—1 oscillation, 1 s, 10 s, 60 s, and 15 min. The features based on 1 oscillation examine the shortest possible time frame, which in monitoring practice is especially useful for detecting short, rapid vibrations and immediate, high-frequency motions. For features derived from raw signals, a graphical representation of a selected features (the ones which are straightforward to visualize) are given in panel b of Figure 1.

17517648, 0, Downloaded from https://onlinelibrary.wiley.com/doi/10.1002/suco.70315 by Universitätsbibliothek, Wiley Online Library on [09/09/2025]. See the Terms and Conditions (https://onlinelibrary.wiley.com/terms-and-conditions) on Wiley Online Library for rules of use; OA articles are governed by the applicable Creative Commons License

TABLE 2 List of candidate signal features evaluated for sensor data, derived from (a) raw signals and (b) normalized profiles.

Signal feature	Description/definition	References
(a) Features derived from raw signals		
S	Signal Skewness: $S=\frac{1}{n}\sum_{i=1}^{n}(x_i-\bar{x})^3/\left(\frac{1}{n}\sum_{i=1}^{n}(x_i-\bar{x})^2\right)^{\frac{3}{2}}$.	33,34
K	Signal Kurtosis: $K=\frac{1}{n}\sum_{i=1}^{n}(x_i-\bar{x})^4/\left(\frac{1}{n}\sum_{i=1}^{n}(x_i-\bar{x})^2\right)^2$.	33–35
$\overline{S}$	Let S_i be the skewness for each cycle in the signal. Then: $\overline{S}=\frac{1}{n_c}\sum_{i=1}^{n_c}S_i$.	33,34
$\overline{K}$	Let K_i be the kurtosis for each cycle in the signal. Then: $\overline{K}=\frac{1}{n_c}\sum_{i=1}^{n_c}K_i$.	33,34
$N_{\max}$	Number of local maxima M_i of the signal.	35–37
$N_{\min}$	Number of local minima m_i of the signal.	35,38
$\bar{t}_r$	Average rise time from local minima to zero: $\bar{t}_r=\frac{1}{n_c}\sum_{i=1}^{n_c}t_{r;i}$.	39
$\bar{t}_{mM}$	Average rise time from local minima to local maxima: $\bar{t}_{mM}=\frac{1}{n_c}\sum_{i=1}^{n_c}t_{mM;i}$.	39,40
$\bar{t}_f$	Average fall time from local maxima to zero: $\bar{t}_f=\frac{1}{n_c}\sum_{i=1}^{n_c}t_{f;i}$.	39
$\bar{t}_{Mm}$	Average fall time from local maxima to local minima: $\bar{t}_{Mm}=\frac{1}{n_c}\sum_{i=1}^{n_c}t_{Mm;i}$.	39,40
$\bar{t}_{(M)p}$	Average time between successive maxima: $\bar{t}_{(M)p}=\frac{1}{n_c-1}\sum_{i=1}^{n_c-1}t_{(M)p;i}$.	15,40
$\bar{t}_{(m)p}$	Average time between successive minima: $\bar{t}_{(m)p}=\frac{1}{n_c-1}\sum_{i=1}^{n_c-1}t_{(m)p;i}$.	15
$\overline{A}$	average maximum: $\overline{A}=\frac{1}{n_c}\sum_{i=1}^{n_c}M_i$.	15,41
E	absolute energy: $E=\sum_{i=1}^{n}x_i^2$.	15
RMS	root mean square: $\mathrm{RMS}=\sqrt{\frac{1}{n}\sum_{i=1}^{n}x_i^2}$.	15,34,35,42
MD	Median absolute differences: let $\Delta x=\{x_{i+1}-x_i \mid i=1\vert\ldots,n-1\}$. $\mathrm{MD}=\mathrm{median}(\Delta x)$.	15
CF	Crest factor: $\mathrm{CF}=\max M_i/\mathrm{RMS}$.	34,42
SF	Shape factor: $\mathrm{SF}=\mathrm{RMS}/\left(\frac{1}{n}\sum_{i=1}^{n}\vert x_i\vert\right)$.	42
IF	Impulse factor: $\mathrm{IF}=\max M_i/\left(\frac{1}{n}\sum_{i=1}^{n}\vert x_i\vert\right)$.	42
(b) Features derived from normalized profiles		
$\mathrm{CC}_{\max}$	For the normalized profiles of the trigger, y^T, and response signals, y^R, we get $CC_{\max}=\max\{c_k\}$ with $c_k=\begin{cases}\frac{1}{n}\sum_{i=1}^{n-k}\left(y_{i+k}^R-\bar{y}^R\right)\left(y_i^T-\bar{y}^T\right), & k>0\\ \frac{1}{n}\sum_{i=1}^{n+k}\left(y_i^R-\bar{y}^R\right)\left(y_{i-k}^T-\bar{y}^T\right), & k<0\end{cases}$.	34,43
$\overline{d}$	We define the pointwise differences as $d_i=\vert y_i^T-y_i^R\vert$. The mean of the differences between the two profiles is calculated as $\overline{d}=\frac{1}{\lambda_p}\sum_{i=1}^{\lambda_p}d_i$.	44
$\mathrm{sd}(r)_{\mathrm{LOESS}}$	We define the LOESS residuals standard deviation as $\mathrm{sd}(r)_{\mathrm{LOESS}}=\sqrt{\frac{1}{\lambda_p-1}\sum_{i=1}^{\lambda_p}(r_i-\bar{r})^2}$, where $\bar{r}=\frac{1}{\lambda_p}\sum_{i=1}^{\lambda_p}r_i$.	45,46
χ_{LOESS}	Let $\mathrm{sd}(r)_{\mathrm{LOESS}}^R$ and $\mathrm{sd}(r)_{\mathrm{LOESS}}^T$ be the LOESS residuals standard deviation for the normalized profiles corresponding to the response and trigger series respectively. The ratio of standard deviations of LOESS residuals for response and trigger normalized profiles is defined as $\chi_{\mathrm{LOESS}}=\frac{\mathrm{sd}(r)_{\mathrm{LOESS}}^R}{\mathrm{sd}(r)_{\mathrm{LOESS}}^T}$.	45,46

Additionally, we derived four features from normalized profiles, which enable a quantitative comparison between the sensor signal and trigger signal profiles. We denote the normalized profiles of the trigger with y^T and of the response signals with y^R. Finally, a couple of features were based on analyzing residuals arising from a second-order polynomial LOESS smoother applied to the normalized profiles.[32] The span was chosen as $\frac{1}{6}$ of the profile length. The residuals obtained from the difference between the normalized profile and the fitted curve are denoted by r_i, $i=1,\ldots,\lambda_P$.

The features selected for this study draw from those used in biomedical signal processing and condition monitoring: (a) distribution-based features (e.g., S, K, $\overline{S}$, $\overline{K}$) were chosen to characterize signal asymmetry and peakedness; (b) cadence-related features (e.g., $\bar{t}_r$, $\bar{t}_{mM}$, $\bar{t}_f$, $\bar{t}_{Mm}$) were included to capture timing relationships that reflect dynamic response characteristics; (c) amplitude-based features (e.g., RMS, $\overline{A}$, E) were selected for their direct relationship to energy transfer in the structure; (d) form factors (e.g., SF, IF, CF) were incorporated to give information about signal waveform; and (e) normalized profile features ($\mathrm{CC}_{\max}$, $\overline{d}$, $\mathrm{sd}(r)_{\mathrm{LOESS}}$) were reported to enable direct comparisons between response and reference signals. This comprehensive

17517648, 0, Downloaded from https://onlinelibrary.wiley.com/doi/10.1002/suco.70315 by Universitätsbibliothek, Wiley Online Library on [09/09/2025]. See the Terms and Conditions (https://onlinelibrary.wiley.com/terms-and-conditions) on Wiley Online Library for rules of use; OA articles are governed by the applicable Creative Commons License

set allows examination of multiple signal aspects that might serve as effective condition surrogates.

2.3.3 | Estimation of variance components

The sensor measurements are influenced by the noise factors—EMI (E), cable vibration (V) and cable length (L)—causing variations in the derived features. To assess these effects and quantify the resulting uncertainties, a random effect model was developed to determine variance components.[24,47] Since variances depend on design factors—specifically, shaker acceleration (1, 3, and 5 m/s^2) and frequency (5 and 25 Hz)—the model was evaluated for each case, resulting in six separate models. Recall that each case had 24 settings of noise factor combinations.

The measurement result, Y_{ijkr} denotes a feature value for replicate $r = 1,...,R$, obtained for a setting defined by the combination of length of cable $i \in \{1,2,3,4\}$, vibration of cable $j \in \{1,2,3\}$, and EMI $k \in \{1,2\}$. Because of substantial remaining variance heterogeneity, we introduce a further random factor for capturing it. So we deal with the model

$$Y_{ijkr} = \mu + L_i + V_j + E_k + \delta_{ijk} + \varepsilon_{ijkr}, \tag{2}$$

where μ denotes the mean value (for a given frequency and acceleration), which refers to the unknown real value. The main factors L_i, V_j and E_k possess a zero mean and respective variances σ_L^2, σ_V^2 and σ_E^2. These quantities reflect the variability associated with the main effects of the factors. The additional term δ_{ijk} represents variation, which cannot be explained by the main effects. Finally, the term ε_{ijkr} denotes the random error between the replicates for one setting. Differently to the common setup, we allow non-constant variance for the last two terms, δ_{ijk} and ε_{ijkr}, with zero mean. Namely, we consider three different schemes. Starting with the first one (length L drives the patterns), we write $\sigma^2_{\delta,L;i}$ and $\sigma^2_{\varepsilon,L;i}$ for the variance of the aforementioned factors. Thus, we allow different variances of these two random components for different i. The index i stands for one of the four realized cable lengths. Similarly, we introduce $(\sigma^2_{\delta,V;j}, \sigma^2_{\varepsilon,V;j})$ for vibration V and $(\sigma^2_{\delta,E;k}, \sigma^2_{\varepsilon,E;k})$ in case of EMI E. As usual, we assume that all random variables are independent and normally distributed (at least approximately). The aforementioned variance components were estimated using restricted maximum likelihood (REML) in python.[48,49] After having conducted the estimation, we pick among the three competing models (L, V, E) the model with the largest realized likelihood. Moreover, we select the "variance cluster" i as index which maximizes $\sigma^2_{\delta,L;i} + \sigma^2_{\varepsilon,L;i}$, in case the L model exhibited the largest likelihood. If one of the other models "scored", we pick the corresponding j or k, accordingly. Denoted with $\sigma^2_{\delta;\max} + \sigma^2_{\varepsilon;\max}$ the resulting maximum variance. Note that all these variances are replaced by their sample counterparts, delivered by the REML procedure.

With the above model including all the subtle variance patterns, the uncertainties were evaluated by adding the variance components together. This approach ensures that we account for the maximum possible total variability across the noise factor levels.

$$u(Y) = \sqrt{\sigma_L^2 + \sigma_V^2 + \sigma_E^2 + \sigma^2_{\delta;\max} + \sigma^2_{\varepsilon;\max}} \tag{3}$$

All calculations were done as it was already mentioned in Section 2.3.2, with $R = 15$ replicates, corresponding to 15 feature values determined for different time window of 1 oscillation, 1, 10 and 60 s. Note that these windows are placed at the beginning of each single minute within the 15 min long signal. In case of considering the entire 15 min window, we have no replicates. Then the component ε_{ijkr} is removed and less variance components are estimated.

To ensure sensor data is effective in monitoring programs, it is crucial to prioritize features that remain unaffected by noise factors. To do so we further define an S/N ratio which is evaluated herein as a ratio of variation across conditional mean response under influence of design factors and the worst-case uncertainty under noise factors, for every feature. The denominator was evaluated as $\max_{d=1,...,6} u(Y)_d$, as the worst-case standard deviation across the six design factor cases.

$$\text{S/N ratio} = \frac{\text{Variability of marginal means across combinations of design factors}}{\text{Worst-case variation under noise factor conditions}} \tag{4}$$

The rationale behind defining such a S/N metric stems from both signal processing literature and Taguchi

17517648, 0, Downloaded from https://onlinelibrary.wiley.com/doi/10.1002/suco.70315 by Universitätsbibliothek, Wiley Online Library on [09/09/2025]. See the Terms and Conditions (https://onlinelibrary.wiley.com/terms-and-conditions) on Wiley Online Library for rules of use; OA articles are governed by the applicable Creative Commons License

designs in quality engineering.[26,50] As the uncertainty caused by noise factors increases, the S/N ratio decreases, making the feature inappropriate due to its susceptibility to the specific noise factors being studied. Likewise, when the level of uncertainty is reduced in relation to the impact of noise factors, the feature becomes less affected by the specific conditions of the noise factor being studied. A heuristic threshold of 3 was used, as is often also used elsewhere for the S/N to determine suitability.[51]

3 | RESULTS

3.1 | Data acquired

In the experiment, two triaxial accelerometers and one inclinometer are used to sense the motion of the shaker. An additional triaxial accelerometer is placed on the shaking device affecting the cables to measure the vibration frequency. The trigger signal is also retrieved as part of the measurements. As a result, a total of 11 channels (see Table S2). Each accelerometer (triaxial sensor and trigger) is recorded with a sampling frequency of 1 kHz, resulting in 900,000 data points in double precision for each channel for each setting. In contrast, the inclinometer is recorded at 100 Hz, resulting in 90,000 data points in double precision for each setting. The recorded data is stored in a comma-separated value (CSV) file, with the entire dataset occupying approximately 32 GB of storage space. The current study is limited to the analysis of signal data corresponding to accelerometer 21,017 in the *x*-direction and the trigger. The remaining channels of the dataset are outside the scope of this study.

3.2 | Signal morphology based on normalized profiles

The first set of questions aimed toward finding (a) how signal shape and morphology changed under the

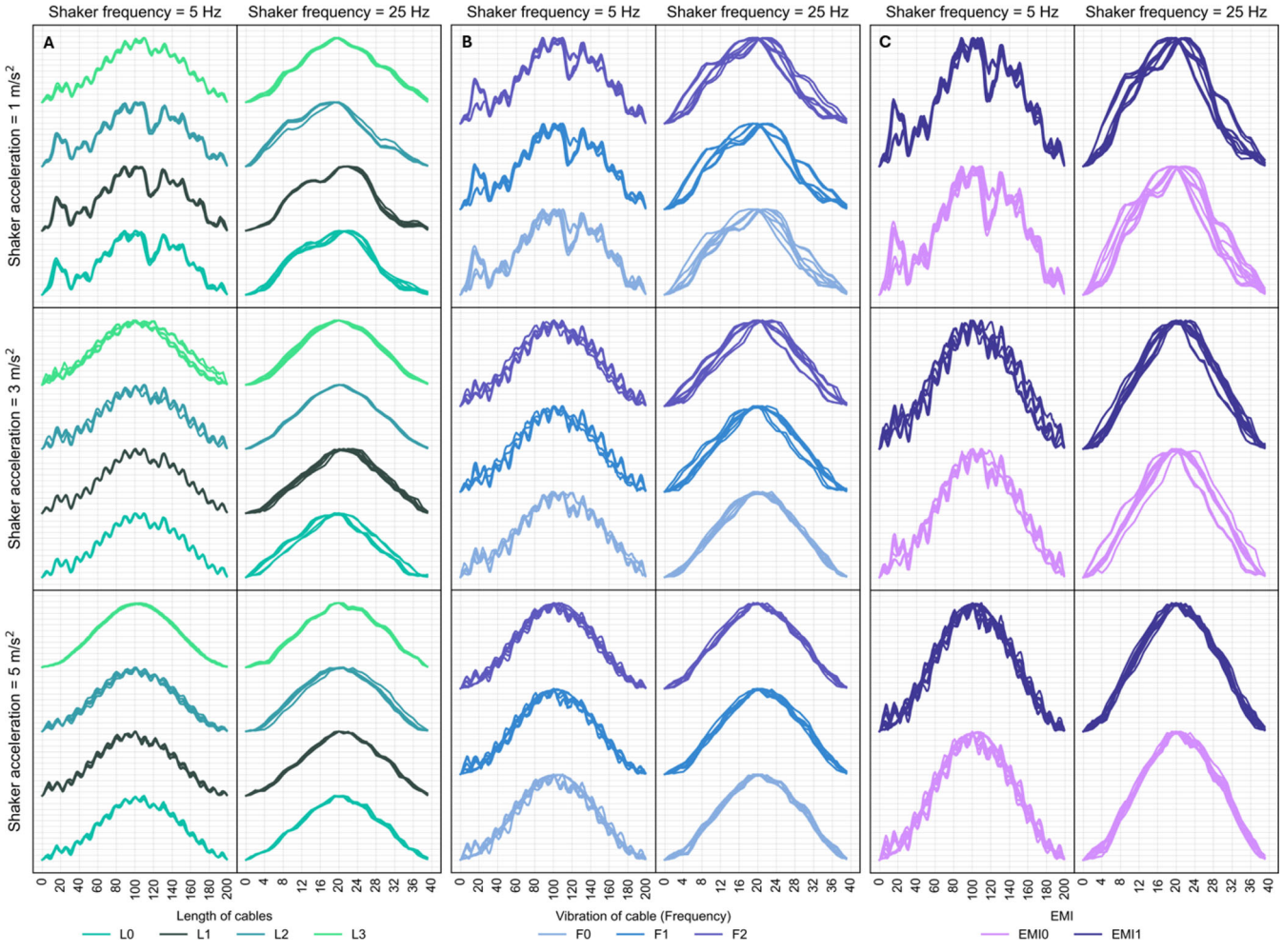

FIGURE 2 Normalized profiles corresponding to accelerometer 21,017 in *x* direction shown in three panels, each with six subplots for combinations of shaker frequency (5 and 25 Hz) in the columns, and shaker acceleration (1, 3 and 5 m/s^2) in the rows. From top to bottom within each subplot, (a) increasing cable lengths of L0 = 25 m, L1 = 50 m, L2 = 75 m, and L3 = 100 m; (b) increasing cable vibration frequencies, F0 = no vibration, F1 = 15 Hz, and F2 = 25 Hz; and (c) with (EMI1) and without (EMI0) electromagnetic interference.

17517648, 0, Downloaded from https://onlinelibrary.wiley.com/doi/10.1002/suco.70315 by Universitatsbibliothek, Wiley Online Library on [09/09/2025]. See the Terms and Conditions (https://onlinelibrary.wiley.com/terms-and-conditions) on Wiley Online Library for rules of use; OA articles are governed by the applicable Creative Commons License

influence of the noise factors and (b) characteristic patterns from the large signal dataset. To facilitate simple and direct comparisons between longer, high-frequency signals, normalized profiles were evaluated. These helped to condense the signal trace and provide a profile to visually and quantitatively compare (a) between different design factor levels and (b) within the noise factor levels.

Figure 2 shows three panels with the normalized profiles, each with subplots for six design factor level combinations juxtaposed together. In each subplot, the color represents the change in noise factor: cable length (shades of cyan-green) in the left panel a, cable vibration (shades of blue) in the center panel b, and EMI (shades of purple) in the right panel c. The different colored profiles are stacked on top of each other. For each color shade plotted, there are 15 normalized profiles, one for each 10-s period of every minute of the 15-min acquisition.

Upon initial examination of the profiles, there are two important takeaways that are readily apparent. First, the accelerometer response exhibits neatly periodic behavior as seen in each subplot; in other words, it demonstrates high "repeatability" over the entire measured duration. The minimal variation in the normalized profiles of the same color across the 15 profiles leads to this conclusion. Second, the shaker conditions in which the sensor was used proved to be more critical, leading to variations in the measurements, that is, the morphology of cycles clearly changed with shaker frequency and acceleration (design factors). This is rather expected behavior.

In contrast to panel a, where the morphologies of the profiles do change with cable length, panels b and c show that the morphological characteristics of the profiles cannot be easily associated with different levels of cable vibration and EMI, respectively. Thus, it can be concluded that the impact of cable vibration or EMI is less visually noticeable on the shape of profiles in comparison to the impact of cable length. Upon closer examination, it is noteworthy that there is a clear change observed due to the changing cable length. The profiles corresponding to a shaker frequency of 5 Hz in panel a prominently show high-frequency patterns. Considering the combination of 5 Hz and 1 m/s^2, there are peaks around index of 20 and troughs around index of 120, which behave very differently for the four cable lengths. Similarly, for the combination of 25 Hz and 1 m/s^2, the shape changes with regard to inflection points around index of 16, with increasing cable length. Turning to combination of 5 Hz and 5 m/s^2, where profiles corresponding to higher cable length exhibit a sinusoidal shape, distinctly different from the others. Thus, the largest change occurred for larger cable lengths; however, it is not completely clear why longer cable length measurements led to such sinusoidal-like shape. Parallel effects due to changing vibration frequency of cable or influence of EMI also are unable to directly explain these effects.

Overall, one can gather several such observations from each subplot, but it is to be underlined that such profiles can help detect variations in vibration signatures, whether caused by noise factors as investigated here or potentially other sources of variability on a bridge. In real-world monitoring circumstances, it is not always possible to collect naturally occurring periodic signals, as can be observed in controlled laboratory experiments. However, other forms of "cycles" or segments of interest can nevertheless be derived from which normalized profiles can be evaluated. For instance, downsampled data over days or weeks would show cyclic behavior, which is changing over different seasons, or events corresponding to multi-axle vehicular traffic. To facilitate studies of such events of interest, normalized profiles are well-suited to assist in formulating pertinent questions and observing the impacts.

Having visually assessed the shape or structure of the normalized profiles, the following section shifts to their quantitative assessment. Despite the distinct appearance of the cycle shape, it is not possible to directly determine if these differences are muddled (occurring by chance) or significant through direct examination. For the above-mentioned two reasons, we continued our pursuit of additional features that can be descriptive of signal patterns.

3.3 | Dispersion of signal features under influence of noise factors

By drawing comparisons to biosignal monitoring[52] where patterns and features are surrogates for physiological parameters (analogous to structural conditions) assisting in diagnostic (analogous to damage detection or identification) or therapeutic (analogous to repairs or maintenance) decision making, the examination of shape and morphology can provide insights into the impact of noise factors on sensor results. Here we proceed to study how the noise factors affect the dispersion of 19 different time-domain signal features. As indicated by the results in the previous section, the signal exhibited a high level of repeatability. Therefore, we will begin by analyzing the characteristics obtained from shorter time frames, specifically those lasting 1 s.

17517648, 0, Downloaded from https://onlinelibrary.wiley.com/doi/10.1002/suco.70315 by Universitätsbibliothek, Wiley Online Library on [09/09/2025]. See the Terms and Conditions (https://onlinelibrary.wiley.com/terms-and-conditions) on Wiley Online Library for rules of use; OA articles are governed by the applicable Creative Commons License

3.3.1 | Features derived from raw signals

Figure 3 presents the factorial effects charts, showing the dispersion of features derived from raw data separated by design and noise factors for a time window of 1 s. Features are arranged row-wise, while the levels of shaker acceleration and shaker frequency are indicated in the bottom and top horizontal axes, respectively. In each of the three columns, the points are colored based on the three noise factors. Each point in the plot represents the average feature value across the replicates from a setting. Similar to the color scheme for normalized profiles, the colors of the point clouds represent the levels of the corresponding noise factor; namely, first column panels have point clouds in shades of cyan-green for varying lengths of cable (25, 50, 75, and 100 m). Levels of vibration of cable are separated in shades of blue in the second column. Finally, in the third column, the point clouds are differentiated by the levels of EMI in shades of purple. The plots also present

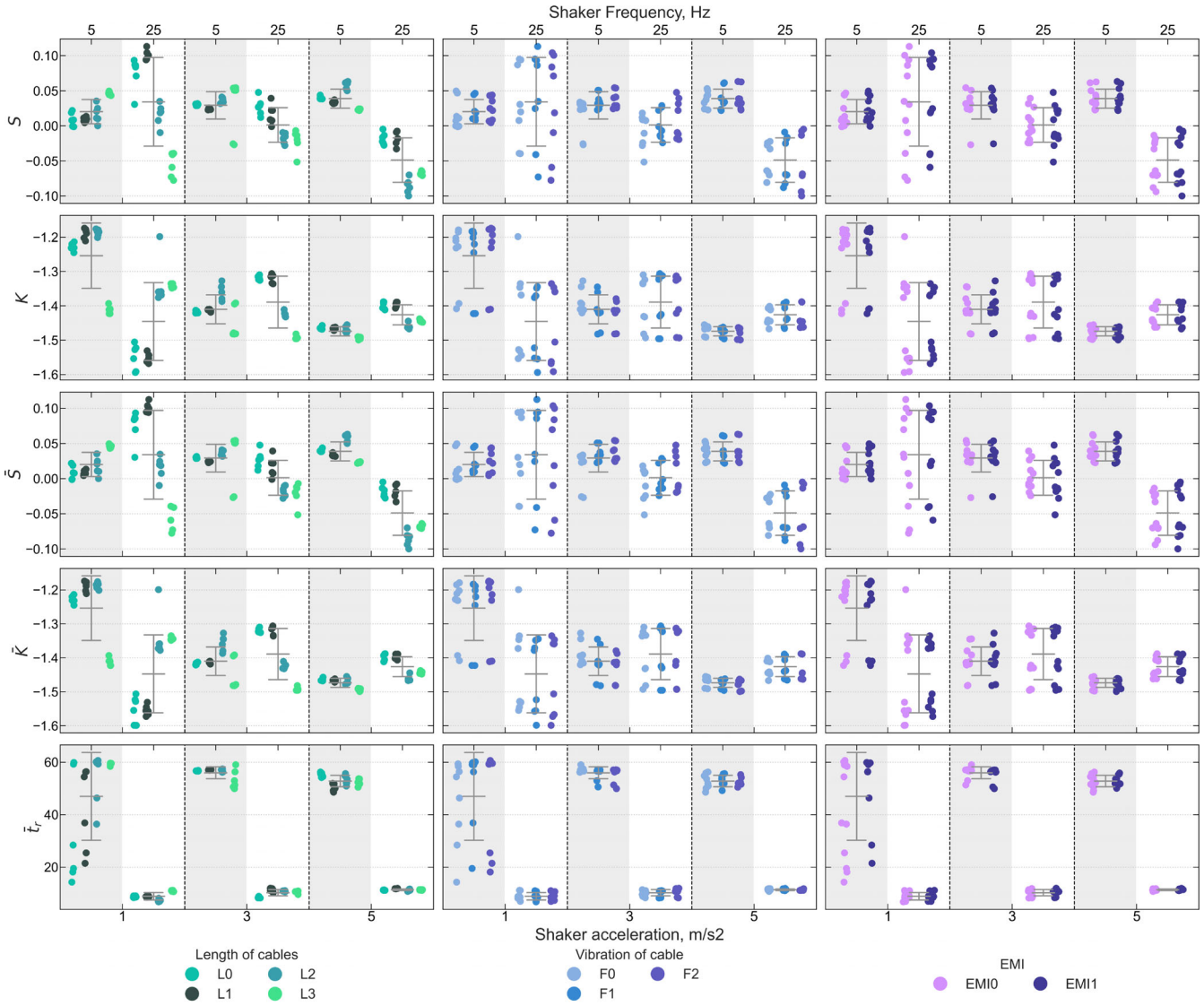

(a)

FIGURE 3 Dispersion of features due to noise factors for different combination of design factors. Each point shows the average feature value for a setting. Points are colored based on the levels of noise factors. Effect of each of the three noise factors can be seen in the three columns. Each subplot is divided into the six cases corresponding to six combinations of shaker acceleration and frequency. Gray line with error bars show mean and standard deviation. (a) Dispersion of four features: S, K, $\overline{S}$, $\overline{K}$ and $\overline{t}_r$ derived from accelerometer signal time window of 1 s. (b) Dispersion of four features: $\overline{t}_{mM}$, $\overline{t}_f$, $\overline{t}_{Mm}$, $\overline{A}$ and E derived from accelerometer signal time window of 1 s. (c) Dispersion of four features: RMS, MD, CF, SF and IF derived from accelerometer signal time window of 1 s.

17517648, 0, Downloaded from https://onlinelibrary.wiley.com/doi/10.1002/suco.70315 by Universitätsbibliothek, Wiley Online Library on [09/09/2025]. See the Terms and Conditions (https://onlinelibrary.wiley.com/terms-and-conditions) on Wiley Online Library for rules of use; OA articles are governed by the applicable Creative Commons License

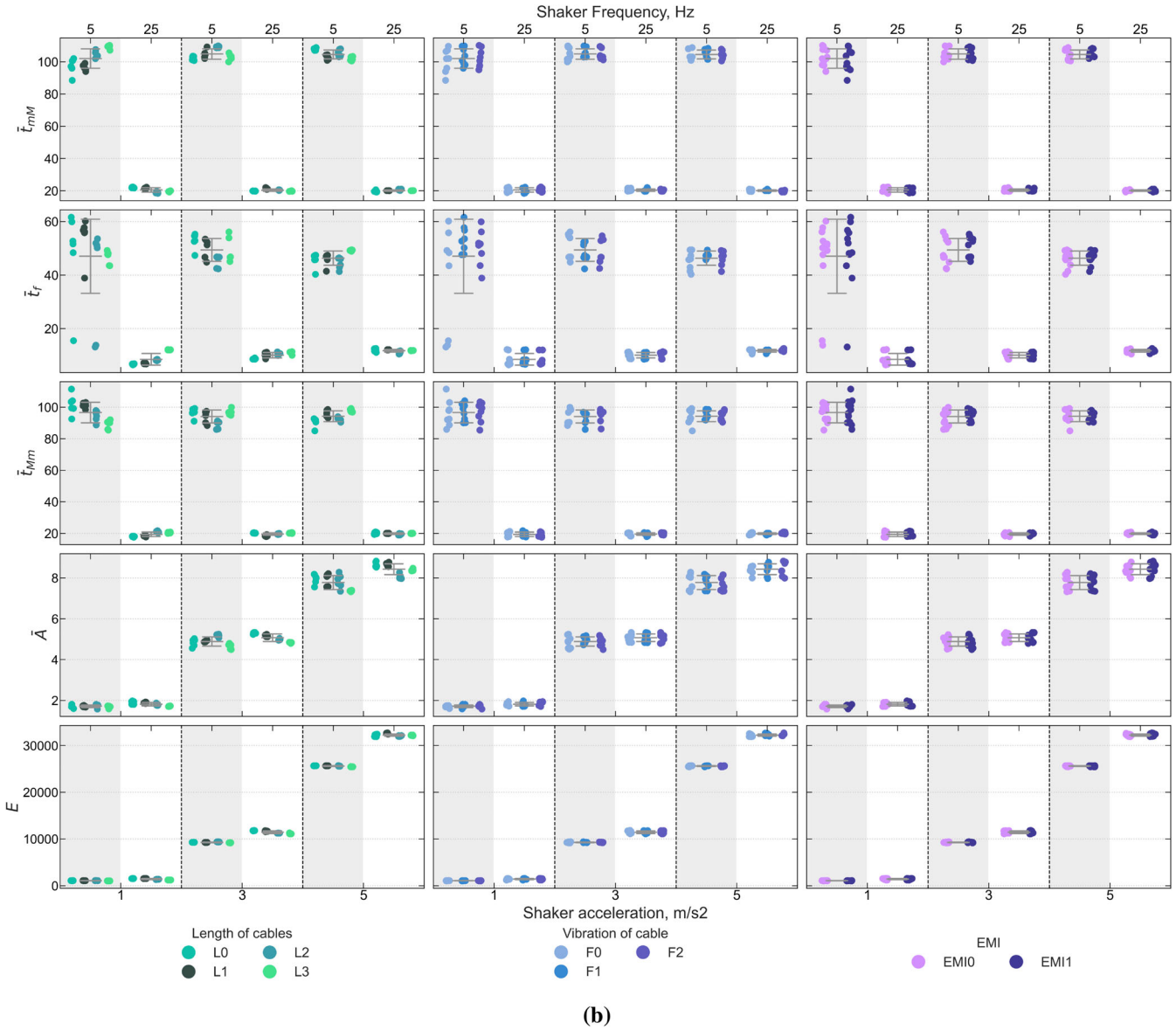

(b)

FIGURE 3 (Continued)

the mean and standard deviation for each combination of design factors.

Fifteen features are plotted across three panels (a) showing S, K, $\overline{S}$, $\overline{K}$, and $\bar{t}_r$, (b) showing $\bar{t}_{mM}$, $\bar{t}_f$, $\bar{t}_{Mm}$, $\overline{A}$, and E, and (c) showing RMS, MD, CF, SF, and IF. Since the dispersion of the remaining four features (N_{max}, N_{min}, $\bar{t}_{(M)p}$, and $\bar{t}_{(m)p}$) is minimal, their plots are included in Figures S5, S6, S11, and S12 respectively. One can learn a lot about the behavior of features by poring over the three panels of such information-heavy charts.

The first observations on the results show the following. By directly comparing between features, on one hand, some of them have very large dispersion, across all design factor cases (e.g., SF, S and $\overline{S}$, K, and $\overline{K}$), even though they are derived from the same signal data, under the same noise factor settings. On the other hand, some other features have very narrow distribution (low dispersion) across all design factor cases (e.g., RMS, E). Features such as $\overline{A}$ and MD have low dispersion for some of the cases, relative to others. For instance, they vary less for both $1\,m/s^2$—5 Hz and $1\,m/s^2$—25 Hz combinations, compared to other cases.

Additionally, two patterns to observe are (i) effect of increasing shaker frequency from 5 to 25 Hz, for a given shaker acceleration and (ii) increasing acceleration, for a given frequency. For the first one, cadence-related features such as $\bar{t}_{mM}$, $\bar{t}_f$, $\bar{t}_{Mm}$, and $\bar{t}_r$ have low dispersion for higher shaker frequency. For instance, at 5 Hz, the standard deviation is approximately 6.7 for the rise time and 7.4 for the fall time, which drops to around 1.4 at 25 Hz.

17517648, 0, Downloaded from https://onlinelibrary.wiley.com/doi/10.1002/suco.70315 by Universitätsbibliothek, Wiley Online Library on [09/09/2025]. See the Terms and Conditions (https://onlinelibrary.wiley.com/terms-and-conditions) on Wiley Online Library for rules of use; OA articles are governed by the applicable Creative Commons License

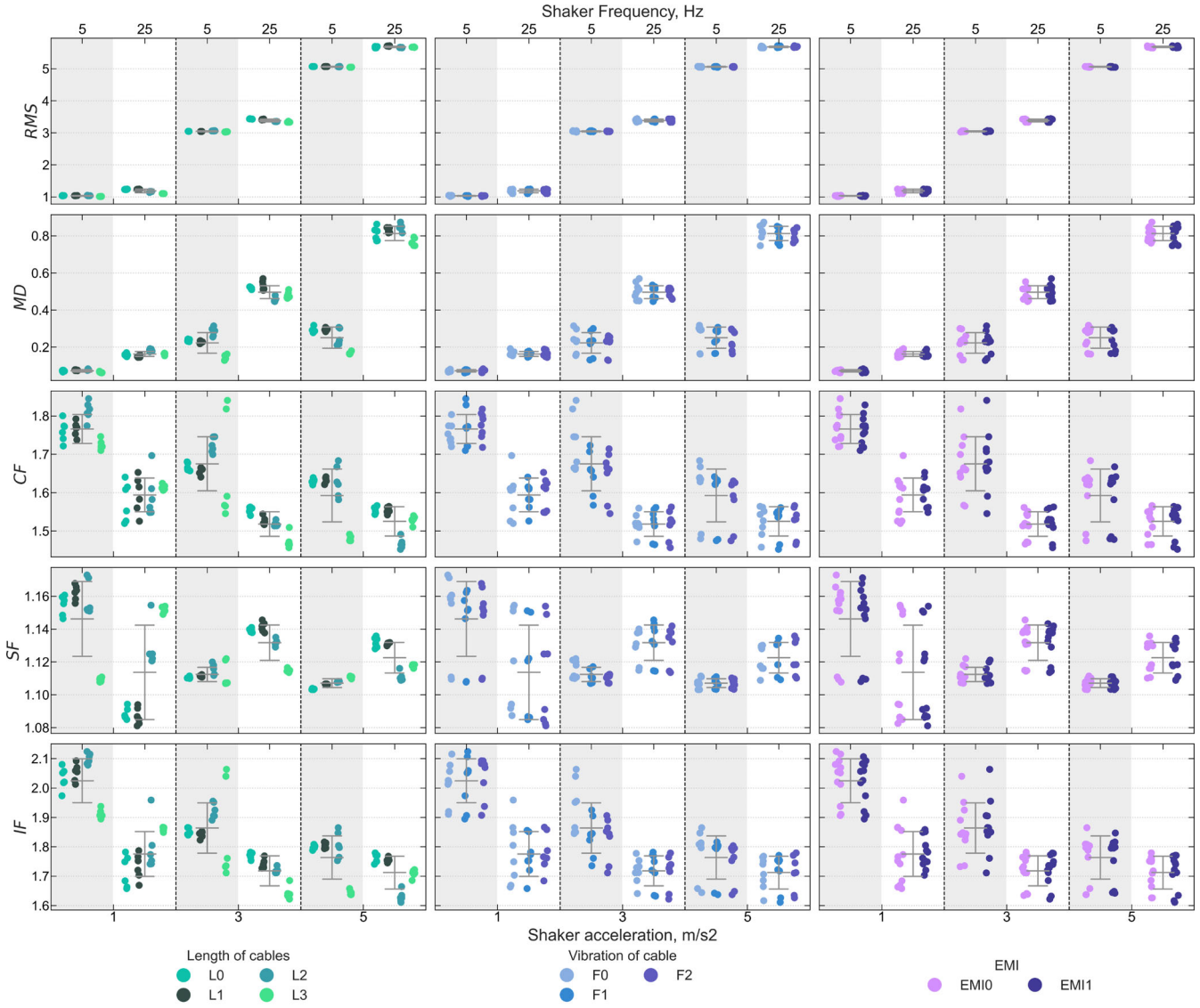

(c)

FIGURE 3 (Continued)

The average values were also lower for the higher shaker frequency. While amplitude related features such as E, RMS, $\overline{A}$, and MD had larger average values for higher shaker frequency. And there was tendency of decreasing dispersion from 5 to 25 Hz. For CF and IF, the average value is lower for the higher frequency compared to the lower one. These observations are entirely consistent with the definitions of the discussed features (see Table 2) and are expected to occur with a higher frequency. Turning to the second pattern. RMS, MD, and $\overline{A}$ tend to linearly increase with increasing shaker acceleration (for both shaker frequencies). We further examined these aspects of linearity in another related work.[22] Feature E also increases with shaker acceleration, perhaps quadratically. Again, one can argue that these observations are unsurprising given how the feature is evaluated. It is noteworthy that while the aforementioned observations are rational and expected, it is remarkable to observe that they still exhibit this behavior even under the influence of noise factors.

Next we look at how average values (gray horizontal lines) are behaving for some specific design factor level cases. Observing the relationship between the average values of S and $\overline{S}$ and the shaker frequency, we see a shift in their tendency upon changing shaker accelerations. An increase in the shaker frequency results in a corresponding increase in the mean value, for acceleration of 1 m/s^2. However, when the shaker frequency increases, there is a decrease in average value for both 3 and 5 m/s^2. Regarding K and $\overline{K}$, along with SF, there is a reversal of

17517648, 0, Downloaded from https://onlinelibrary.wiley.com/doi/10.1002/suco.70315 by Universitätsbibliothek, Wiley Online Library on [09/09/2025]. See the Terms and Conditions (https://onlinelibrary.wiley.com/terms-and-conditions) on Wiley Online Library for rules of use; OA articles are governed by the applicable Creative Commons License

these observations. Nevertheless, for these three features, the lowest acceleration showed the differential tendency. The consistency between S and $\overline{S}$, K and $\overline{K}$, evident in the spread of point clouds in the charts shows that periodic signals remained stable.

We now look at specific design factor level cases where dispersion was either very high or very low compared to the others. For instance, $\bar{t}_{\mathrm{f}}$ and $\bar{t}_{\mathrm{r}}$ have very large dispersion for 1 m/s^2—5 Hz combination (standard deviation of 20 in both cases), compared to the other cases. Similarly, S and $\overline{S}$ have large dispersion for 1 m/s^2—25 Hz combination. While, SF, K, and $\overline{K}$ have large variability in feature values for both shaker frequencies at 1 m/s^2, when compared to other cases. On closer observation (looking at color shading), changing noise factor levels do not specifically explain these observations. This large variability is most likely attributable to the presence of higher frequency oscillatory patterns, as observed in the normalized profiles. Furthermore, these observations are intriguing because the experimental campaign's first set of measurements were conducted under these settings, hence, may potentially be attributed to a "learning effect" on the part of the human conducting the experiment. Such aspects are "natural" and can also occur on a bridge.

Moving next to observing the "main effects" of the three noise factors. For the effect of cable length we look at the first column of all plots of Figure 3 with cyan-green shaded points. For all the features, we observe that on changing the cable length from 25 m to 100 m, the point cloud dispersion shifts. This is visually pronounced, for several features, for example, S, $\overline{S}$, K, $\overline{K}$, $\bar{t}_{\mathrm{r}}$, $\bar{t}_{\mathrm{mM}}$, $\bar{t}_{\mathrm{f}}$, $\bar{t}_{\mathrm{Mm}}$, among others. It is not easy to determine if these characteristics tend to increase or decrease with increasing or decreasing cable lengths. However, the point cloud data suggests that this noise factor does have an impact on the features. Furthermore, it is noteworthy that the features exhibit minimal variability for the longest cable length, in contrast to the variability observed for other cable lengths. This is elaborated upon later in the next section.

Two cadence features: $\bar{t}_{\mathrm{mM}}$ and $\bar{t}_{\mathrm{Mm}}$ demonstrate significantly less dispersion, compared to $\bar{t}_{\mathrm{r}}$ and $\bar{t}_{\mathrm{f}}$. At an acceleration of 1 m/s^2 and a frequency of 5 Hz, there are positive and negative trends with increasing cable length for $\bar{t}_{\mathrm{mM}}$ and $\bar{t}_{\mathrm{Mm}}$, respectively.

For cable vibration and EMI, there are comparatively smaller effects that can be seen in the plots, in the second and third column subplots, respectively. However, some features do reflect shifts in data points due to cable vibration. For instance, with SF, IF, and CF one can notably see at 3 m/s^2 and 5 Hz, that data points for which no vibration was applied, are on average higher than the case with vibration. Effect of cable vibration can also be seen for feature subplots corresponding to S, $\overline{S}$, K, $\overline{K}$, $\bar{t}_{\mathrm{r}}$.

To examine the effect of EMI, for each combination of design factor levels, we see that barring exceptions for S, $\overline{S}$, K, $\overline{K}$, $\bar{t}_{\mathrm{r}}$, where insignificant shifts in distribution are seen, the point clouds are (nearly) equally distributed when EMI is switched off and on. As it was already pointed out, this consistent distribution indicates that the main effect of that noise factor is not considerable.

So far the results reveal that (i) there are some factors which tend to be affected by noise factors, and some which are not, meaning that the features are insensitive to noise factors, and (ii) there are additional effects that cannot be explained by the main effects from the noise factors. We explore this aspect further in the next section.

3.3.2 | Time and setting related variability

So far all the results have been discussed for the case where they were derived using a time window of 1 s. We explore the question whether there are any short term or long term variabilities. Figure 4 exemplarily shows the feature $\bar{t}_{\mathrm{Mm}}$ for four time windows, presented row-wise. What is immediately clear is the similarity of the scatter pattern between different time windows. This is also noticeable when the scatter patterns corresponding to the influence of the length of cables are compared, where we expect the data points to shift due to increasing cable length. This indicates that the duration of the time window has less influence on the investigated time-domain features. We see that it is not necessary to calculate an average value over a longer period for many features, because the same information may already be derived from a shorter duration. This also verifies that the sensor signal had nearly the same pattern across a 15-min period, something that we observed by looking at the normalized profiles as well. We refer the reader to Figures S1–S19 in order to see similar charts for the remaining features. As a result, it is possible to deduce a full sequence of features with a quite high level of accuracy. The reason for this is that the purported repetition error is negligible in comparison to temporal fluctuations and systematic errors, such as those caused by variations in cable length.

The reader may question the necessity of certain features, as they may be redundant, or the calculation of certain features at five different time intervals. However, the current findings suggest that distinct features can display different responses under design and noise factor settings, and that long-term variability is not substantial. These conclusions could not have been reached without studying them in this manner.

17517648, 0, Downloaded from https://onlinelibrary.wiley.com/doi/10.1002/suco.70315 by Universitätsbibliothek, Wiley Online Library on [09/09/2025]. See the Terms and Conditions (https://onlinelibrary.wiley.com/terms-and-conditions) on Wiley Online Library for rules of use; OA articles are governed by the applicable Creative Commons License

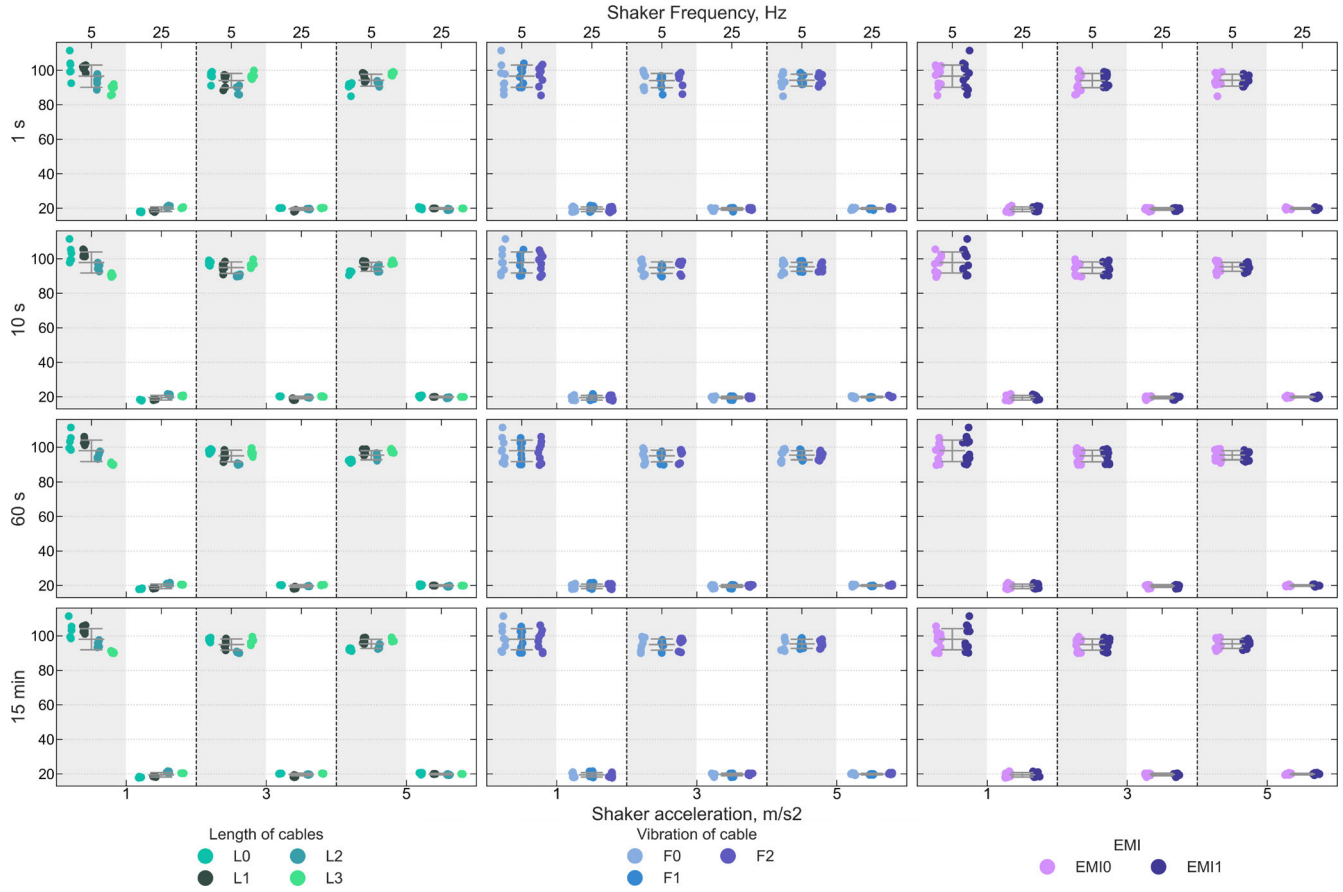

FIGURE 4 Dispersion of $\bar{t}_{\mathrm{Mm}}$ due to noise factors for different combination of design factors evaluated for four time windows—1 s, 10 s, 60 s, and 15 min. Each point shows the average feature value for a setting. Points are colored based on the levels of noise factors. Gray line with error bars show mean and standard deviation.

An interesting finding was made earlier regarding additional effects that cannot be explained by the main effects of the noise factors. These additional effects may manifest as interaction effects among the three noise factors or may be caused due to unintended external sources that affect the measurements, such as human and time effects. To shed light on this, we shift gears and look at the data from a different perspective so as to reveal these "interaction effects".

Figure 5 shows four factors, namely, CF, SF, $\bar{t}_{\mathrm{r}}$, and $\bar{t}_{\mathrm{mM}}$ derived for time window of 1 s. These are evaluated for 1 m/s^2—5 Hz combination of design factor. In each panel we see 24 elapsed time points corresponding to the 24 settings of noise factors. Marker shapes of circle, square and diamond show the three levels of cable vibration frequency, and shades of purple show EMI. The cable length is shown with separation highlighted in the plot, that is, first six points correspond to 25 m, the next six for 50 m and so on. For each marker, there are small gray dots that also show the replicates. In this view of the data, we see all the data points at very granular level. The data reveals that SF has very little variation between the replicates, while $\bar{t}_{\mathrm{r}}$, and $\bar{t}_{\mathrm{mM}}$ show large variation between replicates (at least for some settings). The presence of heteroscedasticity, as noted before, is evident in this case, indicating that the assumptions made in the modeling process were valid. Significant drop is observed while transitioning from a cable length of 75 to 100 m when examining SF. Similarly, jumps are seen within 25 m for $\bar{t}_{\mathrm{r}}$ when EMI is switched on. All these aspects convey presence of strong interplay between the noise factors. Additionally, there is evidence suggesting that because the 100 m cable setups were conducted near the end of the experimental campaign, some external factors might be affecting the results. In retrospect, it is possible that this situation could have been prevented by implementing further randomization. However, doing so would have required additional effort from the human researcher and may have resulted in more errors, all while considering the limitations imposed by practical constraints (e.g., connecting and disconnecting multiple, long cable spools). The results indicate the presence of additional variance components, beyond the main effects, which were appropriately accounted for in the model (see Equation 2).

17517648, 0, Downloaded from https://onlinelibrary.wiley.com/doi/10.1002/suco.70315 by Universitätsbibliothek, Wiley Online Library on [09/09/2025]. See the Terms and Conditions (https://onlinelibrary.wiley.com/terms-and-conditions) on Wiley Online Library for rules of use; OA articles are governed by the applicable Creative Commons License

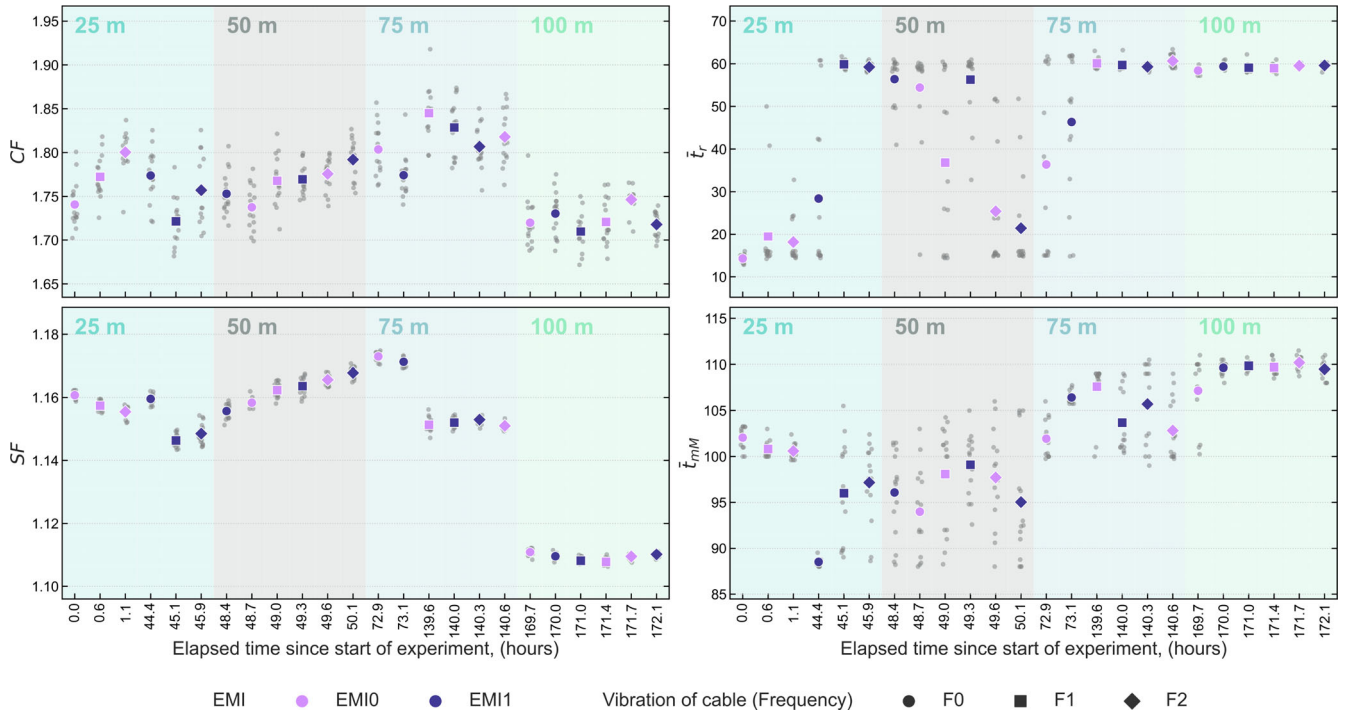

FIGURE 5 Results for 24 settings for four features arranged chronologically since the beginning of the experiment, derived for time window of 1 s. The values are for one case of design factor level combination (1 m/s^2—5 Hz) Bigger markers show average of the 15 replicates (gray dots). EMI is colored in shade of purple. Marker shape shows cable vibration levels. Shaded sections of the subplot show the cable length levels.

While we observed consistent anomalies in the 100 m cable length measurements conducted during the final days of testing, we cannot provide specific evidence for the exact external factors responsible for this behavior. These anomalies may have resulted from unidentified environmental changes, experimental setup variations, operator fatigue, or equipment aging effects that were not captured in our formal experimental design. This limitation highlights the challenge of controlling all variables in extended measurement campaigns. Despite this limitation, the observed anomalies provide valuable insight into real-world monitoring challenges where unexplained variations commonly occur.

3.3.3 | Features derived from normalized profiles

Moving to evaluating a set of quantitative features for normalized profiles. Figure 6 shows these features once again separated by design and noise factors, in a similar fashion as seen previously. The objective is to conduct a quantitative evaluation of normalized profiles while simultaneously testing and confirming our own methodologies.

The CC_{max} feature exhibits distinct behavior across various experimental conditions. Firstly, values obtained at a shaker frequency of 5 Hz are consistently higher compared to those at 25 Hz. This discrepancy can be attributed to differences in the length of normalized profiles between the two frequencies. For 5 Hz there is a tendency of increasing values with higher shaker acceleration. Interestingly, when examining the effect of cable length, a distinct pattern emerges particularly at 5 Hz. Here, an increase in the maximum cross correlation values is observed with longer cable lengths, while other noise factors show negligible impact.

$\overline{d}$ feature exhibits a decrease in its mean values as the shaker acceleration increases. Secondly, the point clouds reveal distinct clusters based on the length of the cable, particularly noticeable for the 100 m length, where we have, in some cases a complete separation from the rest of the points. This clustering effect highlights the influence of cable length on these features. In contrast, other noise factors do not significantly differentiate the points, suggesting that cable length is the primary factor affecting the clustering pattern.

The $\mathrm{sd}(r)_{\mathrm{LOESS}}$ feature exhibits a decreasing trend with increasing acceleration, with a more pronounced decrease observed at a frequency of 5 Hz. Notably, if we explore the effect of the cable length, at 5 Hz we see that the points associated to 100 m are distinctly separated from the others. This separation, coupled with a reduction in residuals, indicates a better LOESS fit in this

17517648, 0, Downloaded from https://onlinelibrary.wiley.com/doi/10.1002/suco.70315 by Universitätsbibliothek, Wiley Online Library on [09/09/2025]. See the Terms and Conditions (https://onlinelibrary.wiley.com/terms-and-conditions) on Wiley Online Library for rules of use; OA articles are governed by the applicable Creative Commons License

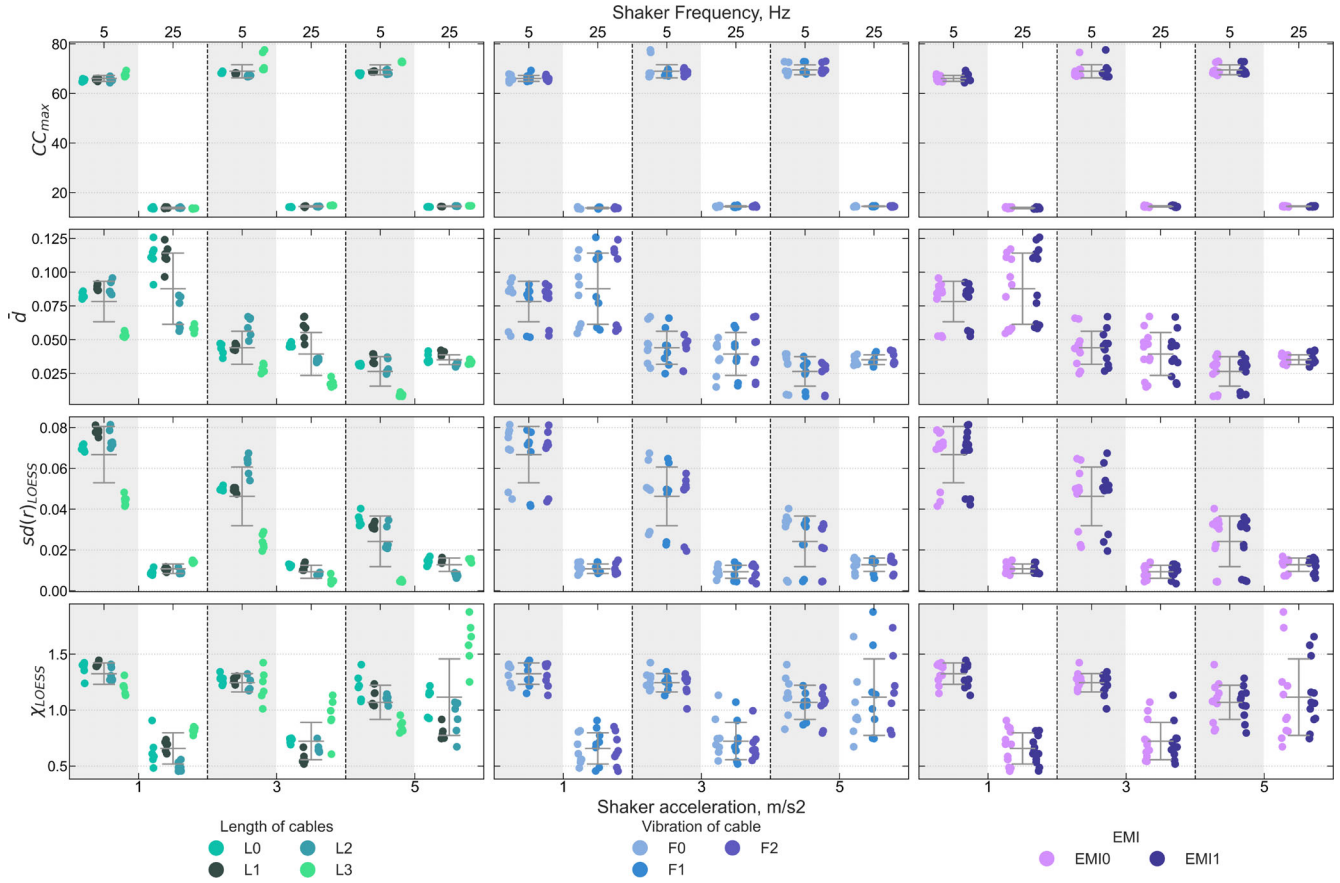

FIGURE 6 Four normalized profile related features and their dispersion due to noise factors for different combination of design factors. Each point shows the average feature value for a setting, that are colored based on the levels of noise factors. Effect of each of the three noise factors can be seen in the three columns. Each subplot is divided into the six cases corresponding to six combinations of shaker acceleration and frequency. Gray line with error bars show mean and standard deviation.

scenario. Consistently, other noise factors show little to no significant effect. Of particular interest is the behavior at an acceleration of 3 m/s^2 and a frequency of 5 Hz, where the points for both the 100 and 75 m cable lengths separate from the remaining data points.

Finally, χ_{LOESS} demonstrates the point distributions corresponding to different shaker frequencies (5 and 25 Hz) are not overlapped for 1 and 3 m/s^2. However, that is not the case for 5 m/s^2, where the distributions for 5 and 25 Hz coincide. At a frequency of 25 Hz and an acceleration of 5 m/s^2, some points separate from the main distribution. Interestingly, these points correspond to the 100 m cable length.

3.4 | Effect of noise factors on signal features

Having now looked at all the features, the results suggest that there has been a clear association between the chosen noise factors and sensor outcomes. The cables between the sensor and DAQs seem to be an important contributor to the MU. On increasing the cable length, we saw changes in signal morphology and in the signal features. Arguably, the revelation of identifying such effects due to cable length is fascinating. Previously reported work on the study of cable length did not report such strong effects, perhaps because the effect was confounded due to another factor or it was studied in a different setup, for example, with smaller cable lengths.[53,54] Furthermore, it was discovered that the 100 m cable experiments, conducted during the final days of the experimental campaign, may have been influenced by unwanted factors warranting additional investigation (see Figure 5). This anomaly suggests the presence of an external source of variation that could be overshadowing or impacting the measurements taken during that period. Such aspects are expected on a bridge as well where not all sources of variability can be controlled or measured. It is critical that efforts are directed to pinpoint the root causes of the effects we have seen by performing confirmation experiments in the future. By effectively

17517648, 0, Downloaded from https://onlinelibrary.wiley.com/doi/10.1002/suco.70315 by Universitatsbibliothek, Wiley Online Library on [09/09/2025]. See the Terms and Conditions (https://onlinelibrary.wiley.com/terms-and-conditions) on Wiley Online Library for rules of use; OA articles are governed by the applicable Creative Commons License

managing and mitigating this source of uncertainty, it is possible to decrease the MU associated.

Further, statistical evidence indicates that cable vibrations do contribute to MU in a limited way. This means that the impact of vehicular traffic or heavy load conditions, which can induce cable vibrations, to the tone of 25 Hz, appears to be minor. It nonetheless represents a non-negligible source of uncertainty. This suggests that while not the primary factor, such vibrations can still meaningfully affect the precision of our measurements.

EMI up to 25 $\mu W/cm^2$ has little to no contribution to the MU. This means that impact of cell towers and exposure to the corresponding level can be considered negligent. However, impact of exposure over larger timescales (e.g., days, months) cannot be discounted.

What stands out from the above is that the careful selection of design and noise factors proved to be highly advantageous, as it facilitated the observation of variations in the sensor response. If measurements were done without the factorial technique, there would be a lack of clarity regarding their source of variation. Furthermore, the learnings from current noise factors enable judicious selection of factors for future experiments. For instance (a) possible role of cable-related factors and (b) limited role of EMI. Lastly, while acknowledging that the impact of cable length on signal response warrants further investigation, we believe that the methodologies employed for uncertainty quantification have proven to be highly effective.

3.5 | Suitability of signal features using S/N ratios

After examining the distribution of feature values in detail, it is evident that there are numerous potential patterns of feature behavior under the influence of noise factors. Some of the behavioral patterns include—(i) consistent smaller or larger variations across all combinations of design factor levels, (ii) significant variations in certain design factor cases, (iii) linear or quadratic increases with shaker acceleration, and (iv) increasing or decreasing tendencies with shaker frequency. In light of these observations, the question arises of how to directly find robust features. A robust feature is one that can retain its information value under various conditions of noise factors. For this, we quantify the uncertainties using Equation (3) and find the maximum (worst-case) uncertainty across the six design factor cases. This value is plugged into Equation (4) along with the variation of a mean value to give the S/N ratio. The approach proposed here is different from the information theory perspective on finding damage-sensitive features by estimating complexity measures.[55,56]

Table 3 shows the S/N ratios obtained for features based on raw signal, evaluated for different time windows. Four of the 19 features are excluded from the table: $N_{\max}$, $N_{\min}$, $\bar{t}_{(M)p}$, and $\bar{t}_{(m)p}$, because variance components could not be estimated for some design factor level cases. Features for which the time window was too small

TABLE 3 S/N ratios for raw signal features evaluated for different time windows.

Feature	1 oscillation	1 s	10 s	60 s	15 min
E	63.510	38.869	36.510	36.606	34.218
RMS	27.8644	29.078	29.094	29.059	29.078
$\overline{A}$	6.214	6.210	6.500	6.444	6.546
$\bar{t}_{\mathrm{mM}}$	*	5.548	5.650	5.601	5.781
$\bar{t}_{\mathrm{Mm}}$	*	4.524	5.106	5.107	5.280
MD	3.261	3.476	3.649	3.635	3.785
$\bar{t}_{\mathrm{r}}$	*	0.937	0.938	0.970	1.006
$\bar{t}_{\mathrm{f}}$	*	0.883	0.992	1.002	1.005
IF	0.731	0.694	0.694	0.696	0.618
CF	0.701	0.668	0.672	0.673	0.593
K	0.557	0.556	0.556	0.555	0.556
$\overline{K}$	*	0.553	0.552	0.552	0.553
$\overline{S}$	*	0.453	0.454	0.453	0.448
S	0.446	0.453	0.453	0.453	0.448
SF	0.443	0.441	0.441	0.443	0.443

Note: Features are sorted in descending order based on the values for 1 s. A higher value of the S/N ratio is better. The cells indicated with an asterisk were not suitable for its calculation.

17517648, 0, Downloaded from https://onlinelibrary.wiley.com/doi/10.1002/suco.70315 by Universitätsbibliothek, Wiley Online Library on [09/09/2025]. See the Terms and Conditions (https://onlinelibrary.wiley.com/terms-and-conditions) on Wiley Online Library for rules of use; OA articles are governed by the applicable Creative Commons License

(1 oscillation) to calculate, S/N ratio is shown as an asterisk.

High S/N ratio is desirable, which means that the feature is insensitive to noise factors. In other words, large S/N ratio means that the variation transmitted by changing (a) length of cable, (b) vibration of cable, and (c) adding EMI, are not affecting these features, which will make them suitable to be able to detect changes that are coming from "real sources of interest" such as the ones cause by loading or damaged state. Of the 15 features, 6 of them have S/N ratios above the threshold of three, at all evaluated time windows. Four features have S/N ratios above threshold of five, at all evaluated time windows. And two features have very large S/N ratio ($\gg 10$), namely, RMS and E. Table 4 lists the S/N ratio for the four features based on normalized profiles. Here one feature (CC_{max}) has value above threshold of three.

The S/N ratios are in the same range when comparing those at short time intervals versus those calculated from longer time intervals. This further confirms that the sensor signal exhibited basically the same patterns for a duration of 15 min. Hence, the S/N ratio does not depend on the duration based on which feature was extracted. This is a fascinating result because it allows one to quickly test and re-test signal features under the influence of noise factors on a bridge by recording very short duration measurements.

The catalog of features investigated here is only exemplar and should not be seen as exhaustive, and the exploration of additional features (even in frequency-domain) is advised. Nevertheless, the base rationale for evaluating the S/N ratio and its methodology does not change and serves as a reliable and simple metric for assessing a feature's suitability.

What emerges from the results reported here is that this empirical approach helps to reduce all the variance analysis to a single metric in order to identify suitable features which are robust under noise factor conditions. One can capture sensor data on the bridge under the influence of different conditions, evaluate candidate features, determine variance components, and find out the S/N ratio. We foresee such an approach to be applied in practice to funnel down suitable features in a methodical way for efficient condition information management and discourage feature selection to be done in an ad hoc manner.[57]

TABLE 4 S/N ratios for normalized cycles related features.

Feature	S/N ratios
CC_{max}	5.663
$sd(r)_{LOESS}$	1.572
$\overline{d}$	0.798
χ_{LOESS}	0.388

4 | DISCUSSION

4.1 | On utility of factorial experimental designs and effects of noise factors on accelerometers

In this study, we set out to address the question: Given a specific measured response value, what is the associated variation or uncertainty without precise knowledge of the "on-ground" conditions? To achieve this, it was crucial to characterize the MU of sensor signals influenced by the noise factors studied herein. The importance of finding the effect of noise factors is embodied in part (b) of Axiom IV, which states, *without intelligent feature extraction, the more sensitive a measurement is to damage, the more sensitive it is to changing operational and environmental conditions*.[2] This study systematically varies three noise factors that can be foreseen on a bridge, thereby contributing to our understanding of their effects on accelerometer signals. This knowledge is crucial for civil engineers performing SHM of bridges through either force-response testing[58] or long-term ambient signal monitoring.[59] Nevertheless, other sources of variability, such as technician mounting/installing the sensor, sensor positioning on the bridge, and the surface condition of the concrete, can be addressed in subsequent studies.[22] Undoubtedly, without the FD, discerning the influences of such noise factors affecting the sensing measurements would be challenging. This promising approach thus sets the stage for future research, which could also systematically vary environmental conditions like temperature and humidity—the known Achilles' heel of SHM systems.[60–62]

4.2 | Utility of features describing shape and morphology

In a world abundant with digitized measurement points and computational power, yet constrained by economic and practical limitations, there is an urgent and imminent need to identify which "features" or "patterns" are truly descriptive or diagnostic of a condition on the bridge.

The temporal variogram approach is used to discern the autocorrelation of a signal and identify the patterns to obtain the segments of interest, which are then averaged (robust mean). Hence, the normalized profiles

17517648, 0, Downloaded from https://onlinelibrary.wiley.com/doi/10.1002/suco.70315 by Universitätsbibliothek, Wiley Online Library on [09/09/2025]. See the Terms and Conditions (https://onlinelibrary.wiley.com/terms-and-conditions) on Wiley Online Library for rules of use; OA articles are governed by the applicable Creative Commons License

proposed here can be interpreted as the average shape of the wave over a specific time period. The advantage of obtaining the profile is to (a) visually contrast the morphology of the longer duration signals, (b) derive shape describing features from the trace. Time domain features and the signal trace are not the go-to features for SHM monitoring because finding the sections of interest in the data ocean is a challenging aspect in a real-life scenario. But once sections of interest are identified, one typically must resort to such shape-related features.

It is evident that various signal features respond differently and show different levels of variation; hence, commenting on the MU of the signal cannot be detached from the evaluation of signal features. The uncertainty quantification here has two main implications. First, it helps to understand the capability of the vibrational-based SHM system, and second, it helps to "sieve out" suitable and robust features to derive from signals. A high degree of uncertainty in accelerometer measurements under the influence of different noise factors impedes the detection of characteristics of interest, such as (minor) levels of damage. The S/N ratio embodies this concept in a single metric. Hence, the proposed approach of determining S/N ratios can be used to assess the performance of feature extraction methods and SHM methods, that is, for their validation, that work with suitable features insensitive to other effects on a bridge. Using the S/N ratio, when one obtains several suitable features, one can conduct dimensionality reduction or formal feature independence analysis (e.g., PCA) to identify a minimal set of orthogonal features that maintain monitoring effectiveness while reducing computational demands.

Building upon the work in this study, future work is needed toward the development of an innovative tool. This tool will not only encapsulate the feature extraction, but also evaluate its suitability, thus ensuring practical application by facilitating the automated extraction and rigorous evaluation of features.

4.3 | On approach to determination of MU

In the classical GUM approach to MU, we consider random and systematic components of variation.[63] The systematic component, or bias, is the expected deviation between measured and true values. In bridge monitoring using sensors, the absence of a "true signal value" makes bias generally unknown. Determining and expressing uncertainties becomes particularly challenging in the absence of a true sensor response value, whether for a healthy or damaged state. A pragmatic way around is to treat the bias as a function of measurement conditions, and calculate its variance based on the variability of these conditions. To overcome this daunting task of MU determination, a top-down approach was devised and employed in this study. This method involved collecting data under controlled sources of variation and characterizing the MU based on signal features. This information about uncertainty sensor outcome under practical sources of variability contributes to evaluating the effectiveness and performance of the SHM systems.[64]

Just as defined standards are available in other fields such as analytical and clinical chemistry for ensuring quality and reliability, MU is equally vital in the field of SHM.[65] Currently, the absence of established protocols for the determination of MU in SHM presents a gap that the proposed designs and methodologies aim to fill. These contributions are essential as they form the basis for a robust QA framework and drive standardization efforts within SHM practices.

5 | CONCLUSIONS

A catalog of several signal features was studied based on short and long time windows. A generalized linear model was developed and employed to determine the MU. The methods appeal to the imminent and urgent need for uncertainty quantification in SHM. The cable length appeared to have a large effect on measurement outcomes; at the same time, the interaction between the three noise factors also proved to be a major source of uncertainty in the features. Future outcomes will involve confirmation experiments as well as exploration of frequency-domain features, which generally are more complex to evaluate. Overall, the different components of variability for different time durations (e.g., short term variability), and where the variability is coming from were elucidated.

Reflecting on the implications, the methodologies proposed here for characterization of MU expressed using signal features can be used for any kind of sensing systems deployed on existing or new structures. Because there are so many influencing factors contributing to uncertainty in sensor outcomes, effective experimental designs to gather measurement data, such as the ones proposed here, can have many practical benefits. The results in this work make a strong case for using FD, through which systematic variation of design and noise factors can be done.

By synthesizing the signal features and associated uncertainties, this study notably highlights how S/N

17517648, 0, Downloaded from https://onlinelibrary.wiley.com/doi/10.1002/suco.70315 by Universitätsbibliothek, Wiley Online Library on [09/09/2025]. See the Terms and Conditions (https://onlinelibrary.wiley.com/terms-and-conditions) on Wiley Online Library for rules of use; OA articles are governed by the applicable Creative Commons License

ratios can help to identify which features are suitable in real-world monitoring scenarios under the influence of noise factors. Thus, it assists in examining their reliability by analyzing the measured responses. Engineers can use this methodology to not only study other sources of variability seen on a structure, but also identify the suitability of damage-sensitive features.

Analogous to healthcare practitioners relying on certain fingerprints in biomedical signals, this work proposes that structural operators can also rely on visual and quantitative cues from normalized profiles derived from vibrational sensors. It is observed that features can exhibit varying levels of dispersion, which will likely impact the accuracy of modeling and decision-making processes that depend on them. The awareness of this phenomenon is crucial for structural engineering and asset owners who are using and deploying SHM systems.

ACKNOWLEDGMENTS

This research is funded by dtec.bw—Digitalization and Technology Research Center of the Bundeswehr [project SHM]. Dtec.bw is funded by the European Union—NextGenerationEU. The collaboration partners at the Helmut-Schmidt University/University of the Federal Armed Forces Hamburg are gratefully acknowledged. Open Access funding enabled and organized by Projekt DEAL.

DATA AVAILABILITY STATEMENT

The data that support the findings of this study are available from the corresponding author upon reasonable request.

ORCID

Sylvia Keßler https://orcid.org/0000-0002-1335-1104

REFERENCES

1. Smith S. Digital signal processing: a practical guide for engineers and scientists. Burlington, MA: Newnes; 2003.
2. Worden K, Farrar CR, Manson G, Park G. The fundamental axioms of structural health monitoring. Proc R Soc A: Math Phys Eng Sci. 2007;463(2082):1639–64.
3. Rytter A. Vibrational based inspection of civil engineering structures. 1993.
4. Yan R, Chen X, Mukhopadhyay SC. Structural health monitoring. Cham: Springer; 2017.
5. Eisermann C, Voigt C, Marx S, Kang C. The initial structural health monitoring system of the Nibelungen Bridge Worms. Proceedings of the 11th European workshop on structural health monitoring (EWSHM 2024). Potsdam, Germany: NDT.net; 2024.
6. Cawley P. Structural health monitoring: closing the gap between research and industrial deployment. Struct Health Monit. 2018;17(5):1225–44.
7. Capellari G, Chatzi E, Mariani S. Cost–benefit optimization of structural health monitoring sensor networks. Sensors. 2018; 18(7):2174.
8. Cawley P. A development strategy for structural health monitoring applications. J Nondestruct Eval Diagn Progn Eng Syst. 2021;4(4):41012.
9. Kahrger B, Möller SK, Jonscher C, Grießmann T, Rolfes R. Detectability of structural damage to a lattice tower using eigenfrequencies and Gaussian process regression. NDTnet. 2024; Preprint.
10. Yen GG, Lin KC. Wavelet packet feature extraction for vibration monitoring. IEEE Trans Ind Electron. 2000;47(3):650–67.
11. Wernitz S, Hofmeister B, Jonscher C, Grießmann T, Rolfes R. A new open-database benchmark structure for vibration-based structural health monitoring. Struct Control Health Monit. 2022;29(11):e3077.
12. Jaelani Y, Klemm A, Wimmer J, Seitz F, Köhncke M, Marsili F, et al. Developing a benchmark study for bridge monitoring. Steel Construct. 2023;16(4):215–25.
13. Brownjohn JM, De Stefano A, Xu YL, Wenzel H, Aktan AE. Vibration-based monitoring of civil infrastructure: challenges and successes. J Civ Struct Health Monit. 2011;1:79–95.
14. Roeck GD. The state-of-the-art of damage detection by vibration monitoring: the SIMCES experience. J Struct Control. 2003;10(2):127–34.
15. Buckley T, Ghosh B, Pakrashi V. A feature extraction and selection benchmark for structural health monitoring. Struct Health Monit. 2022;22(3):2082–127.
16. Cicirello A. Physics-enhanced machine learning: a position paper for dynamical systems investigations. J Phys Conf Ser. 2024;2909:12034.
17. Hemez FM, Doebling SW. Model validation and uncertainty quantification. Los Alamos, NM: Los Alamos National Lab. (LANL); 2000.
18. Thacker BH, Doebling SW, Hemez FM, Anderson MC, Pepin JE, Rodriguez EA. Concepts of model verification and validation. 2004.
19. JCGM. International vocabulary of metrology - basic and general concepts and associated terms (VIM) (JCGM 200:2012). Paris, France: Joint Committee for Guides in Metrology (BIPM); 2012.
20. Veluthedath Shajihan SA, Chow R, Mechitov K, Fu Y, Hoang T, Spencer BF Jr. Development of synchronized high-sensitivity wireless accelerometer for structural health monitoring. Sensors. 2020;20(15):4169.
21. Dorst T, Gruber M, Seeger B, Vedurmudi AP, Schneider T, Eichstädt S, et al. Uncertainty-aware data pipeline of calibrated MEMS sensors used for machine learning. Meas Sensors. 2022; 22:100376.
22. Nichani K, San Martin V, Jaelani Y, Frost K, Beering C, Hettwer K, et al. On suitability of measures of amplitude for quality assurance of vibration sensing systems in structural health monitoring. Struct Concr. 2024. https://doi.org/10.1002/suco.70070
23. Sörnmo L, Laguna P. Bioelectrical signal processing in cardiac and neurological applications. Academic Press series in biomedical engineering. Amsterdam, The Netherlands: Elsevier Science; 2005.

17517648, 0, Downloaded from https://onlinelibrary.wiley.com/doi/10.1002/suco.70315 by Universitätsbibliothek, Wiley Online Library on [09/09/2025]. See the Terms and Conditions (https://onlinelibrary.wiley.com/terms-and-conditions) on Wiley Online Library for rules of use; OA articles are governed by the applicable Creative Commons License

24. ISO/TS 23471. ISO/TS 23471:2022 experimental designs for evaluation of uncertainty – use of factorial designs for determining uncertainty functions. Tokyo, Japan: International Organization for Standardization; 2022.
25. Montgomery DC. Design and analysis of experiments. 9th ed. Hoboken, NJ: John Wiley & Sons; 2017.
26. Freddi A, Salmon M. Introduction to the Taguchi method. Design principles and methodologies: from conceptualization to first prototyping with examples and case studies. Cham, Switzerland: Springer; 2019. p. 159–80.
27. Manfred Weber Metra Mess- und Frequenztechnik in Radebeul e K. Piezoelectric accelerometers: Theory and application. 2021. Accessed: May 18, 2024. https://mmf.de/wp-content/uploads/2023/08/transducermane.pdf
28. Aktan AE, Catbas FN, Grimmelsman KA, Pervizpour M. Development of a model health monitoring guide for major bridges (Report No. FHWA-RD-02-042). Washington, DC: Federal Highway Administration, Office of Research and Development; 2002.
29. Zhu L, Fu Y, Chow R, Spencer BF Jr, Park JW, Mechitov K. Development of a high-sensitivity wireless accelerometer for structural health monitoring. Sensors. 2018;18(1):262.
30. Glisic B. Concise historic overview of strain sensors used in the monitoring of civil structures: the first one hundred years. Sensors (Basel). 2022;22(6):2397.
31. Cooley D, Naveau P, Poncet P. Variograms for spatial max-stable random fields. In Dependence in probability and statistics. New York, NY: Springer; 2006. p. 373–90.
32. Uhlig S. The LOESS smoother: incorporation of uncertainty data and the behaviour with missing values. Copenhagen, Denmark: International Council for the Exploration of the Sea (ICES), Working Group on Statistical Aspects of Environmental Monitoring; 2001.
33. Figueiredo E, Park G, Figueiras J, Farrar C, Worden K. Structural health monitoring algorithm comparisons using standard data sets. 2009. https://www.osti.gov/biblio/961604
34. Adams D. Health monitoring of structural materials and components: methods with applications. Hoboken, NJ: John Wiley & Sons; 2007.
35. Zhang H, Lin J, Hua J, Gao F, Tong T. Data anomaly detection for bridge SHM based on CNN combined with statistic features. J Nondestruct Eval. 2022;41(1):28.
36. Miletić M, Atanasoski V, Kršić J, Lazović A, Popović-Maneski L. Validation of the new wearable instrument for the pendulum test based on inertial sensors. In Proceedings 7th international conference IcETRAN. Belgrade, Serbia: IcETRAN; 2020. p. 246–9.
37. Gupta P, Gupta M, Kumar V. An active learning enhanced data programming (ActDP) framework for ECG time series. Machine Learn: Sci Technol. 2024;5:35016. https://doi.org/10.1088/2632-2153/ad5fda
38. Chan-Viquez D, Hasanbarani F, Zhang L, Anaby D, Turpin NA, Lamontagne A, et al. Development of vertical and forward jumping skills in typically developing children in the context of referent control of motor actions. Dev Psychobiol. 2020;62(6):711–22. https://doi.org/10.1002/dev.21949
39. Li W, Luo X, Poetsch MS, Oertel R, Nichani K, Schneider M, et al. Synergistic adverse effects of azithromycin and hydroxychloroquine on human cardiomyocytes at a clinically relevant treatment duration. Pharmaceuticals. 2022;15(2):220.
40. LeMoyne R, Mastroianni T. Visualization of the machine learning process using J48 decision tree for biometrics through ECG signal. J Biomed Sci Eng. 2022;15:287–96.
41. Ahmed N, Rafiq JI, Islam MR. Enhanced human activity recognition based on smartphone sensor data using hybrid feature selection model. Sensors. 2020;20(1):293. https://www.mdpi.com/1424-8220/20/1/317
42. Wang X, Zheng Y, Zhao Z, Wang J. Bearing fault diagnosis based on statistical locally linear embedding. Sensors. 2015;15(7):16225–47. https://www.mdpi.com/1424-8220/15/7/16225
43. Ciminello M, Ameduri S, Romano F, Concilio A. Impact area and debonding line detection assessment by cross-correlation analysis and distributed sensing. Opt Fiber Technol. 2020;58:102245. https://www.sciencedirect.com/science/article/pii/S1068520020302352
44. Bahrani N, Levenberg E, Blanc J, Hornych P. Inverse analysis of pavement layer moduli based on data collected by buried accelerometers and geophones. In: Chabot A, Hornych P, Harvey J, Loria-Salazar LG, editors. Accelerated pavement testing to transport infrastructure innovation. Cham: Springer International Publishing; 2020. p. 592–601.
45. Klanderman MC, Lee J, Villez K, Cath TY, Hering AS. Adaptive online multivariate signal extraction with locally weighted robust polynomial regression. Data Sci Sci. 2023;2(1):2200856. https://doi.org/10.1080/26941899.2023.2200856
46. Clarke DC, Richardson M. The benefits of continuous local regression for quantifying global warming. Earth Space Sci. 2021;8(5):e2020EA001082. https://doi.org/10.1029/2020EA001082
47. Uhlig S, Colson B, Gowik P. Measurement uncertainty interval in case of a known relationship between precision and mean. F1000Res. 2023;12:12.
48. Rao PS. Variance components: mixed models, methodologies and applications. Vol 78. Boca Raton, FL: CRC Press; 1997.
49. Python Software Foundation. Python: a dynamic, open source programming language. 2023 https://www.python.org/
50. Leon RV, Shoemaker AC, Kacker RN. Performance measures independent of adjustment: an explanation and extension of Taguchi's signal-to-noise ratios. Technometrics. 1987;29(3):253–65.
51. O'Haver T. A pragmatic introduction to signal processing. 2023 Accessed May 11, 2024. https://terpconnect.umd.edu/toh/spectrum/
52. Kaniusas E, Kaniusas E. Physiological phenomena and biosignals. Vienna, Austria: Springer; 2012.
53. Kess H, Adams D. Investigation of operational and environmental variability effects on damage detection algorithms in a woven composite plate. Mech Syst Signal Process. 2007;21(6):2394–405.
54. Bartels JH, Gebauer D, Marx S. Einflüsse auf die Messunsicherheit von SHM-Systemen und deren Kompensation am Beispiel von Laser-Distanzmessungen. Bautechnik. 2023;100(2):67–74.
55. Donajkowski H, Leyasi S, Mellos G, Farrar CR, Scheinker A, Pei JS, et al. Comparison of complexity measures for structural health monitoring. In: Barthorpe R, editor. Model validation and uncertainty quantification, volume 3: proceedings of the

17517648, 0, Downloaded from https://onlinelibrary.wiley.com/doi/10.1002/suco.70315 by Universitätsbibliothek, Wiley Online Library on [09/09/2025]. See the Terms and Conditions (https://onlinelibrary.wiley.com/terms-and-conditions) on Wiley Online Library for rules of use; OA articles are governed by the applicable Creative Commons License

38th IMAC, a conference and exposition on structural dynamics 2020. Cham, Switzerland: Springer; 2020. p. 27–39.
56. West BM, Locke WR, Andrews TC, Scheinker A, Farrar CR. Applying concepts of complexity to structural health monitoring. In: Wicks AM, editor. Structural health monitoring, photogrammetry & DIC, volume 6: proceedings of the 36th IMAC, a conference and exposition on structural dynamics 2018. Cham, Switzerland: Springer; 2019. p. 205–15.
57. Worden K, Dervilis N, Farrar C. Applying the concept of complexity to structural health monitoring. In: Chang FK, Guemes A, Kopsaftopoulos F, editors. Proceedings of the 12th international workshop on structural health monitoring: enabling intelligent life-cycle health management for industry internet of things (IIOT), IWSHM 2019. Stanford, CA: DEStech Publications; 2019. p. 3226–34.
58. Helmi K, Taylor T, Ansari F. Shear force–based method and application for real-time monitoring of moving vehicle weights on bridges. J Intell Mater Syst Struct. 2015;26(5):505–16.
59. Bunce A, Brennan DS, Ferguson A, O'Higgins C, Taylor S, Cross EJ, et al. On population-based structural health monitoring for bridges: comparing similarity metrics and dynamic responses between sets of bridges. Mech Syst Signal Process. 2024;216:111501.
60. Han Q, Ma Q, Xu J, Liu M. Structural health monitoring research under varying temperature condition: a review. J Civ Struct Health Monitor. 2021;11:149–73.
61. Keshmiry A, Hassani S, Mousavi M, Dackermann U. Effects of environmental and operational conditions on structural health monitoring and non-destructive testing: a systematic review. Buildings. 2023;13(4):918.
62. Brunner AJ. A review of approaches for mitigating effects from variable operational environments on piezoelectric transducers for long-term structural health monitoring. Sensors. 2023; 23(18):7979.
63. BIPM I, IFCC I, ISO I, IUPAP, OIML. Evaluation of measurement data—guide to the expression of uncertainty in measurement (JCGM 100: 2008 GUM 1995 with minor corrections). Vol 98. Sèvres, France: Joint Committee for Guides in Metrology; 2008.
64. On Structural Health AISC. Guidelines for implementation of structural health monitoring on fixed wing aircraft. Warrendale, PA: SAE International; 2021.
65. Mendler A. SHM Leistungsbewertung durch einen digitalen Zwilling. Fachtagung Bauwerksdiagnose. Berlin: Fachtagung Bauwerksdiagnose; 2024. https://www.ndt.net/?id=29376

AUTHOR BIOGRAPHIES

Kapil Nichani, QuoData GmbH, Dresden, Germany. Email: kapil.nichani@quodata.de.

Steffen Uhlig, QuoData GmbH, Berlin, Germany. Email: steffen.uhlig@quodata.de.

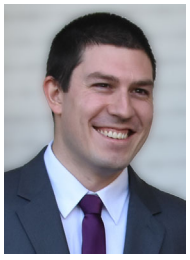

Victor San Martin, QuoData GmbH, Dresden, Germany. Email: victor.san-martin@quodata.de.

Yogi Jaelani, Department of Engineering Materials and Building Preservation, School of Mechanical and Civil Engineering, Helmut Schmidt University Hamburg, Germany. Email: yogi.jaelani@hsu-hh.de.

Kirstin Frost, QuoData GmbH, Dresden, Germany. Email: kirstin.frost@quodata.de.

Carina Beering, Department of Mathematics & Statistics, School of Economic and Social Sciences, Helmut Schmidt University Hamburg, Germany. Email: beeringc@hsu-hh.de.

Karina Hettwer, QuoData GmbH, Dresden, Germany. Email: hettwer@quodata.de.

17517648, 0, Downloaded from https://onlinelibrary.wiley.com/doi/10.1002/suco.70315 by Universitätsbibliothek, Wiley Online Library on [09/09/2025]. See the Terms and Conditions (https://onlinelibrary.wiley.com/terms-and-conditions) on Wiley Online Library for rules of use; OA articles are governed by the applicable Creative Commons License

Sven Knoth, Department of Mathematics & Statistics, School of Economic and Social Sciences, Helmut Schmidt University Hamburg, Germany. Email: knoth@hsu-hh.de.

Sylvia Keßler, Department of Engineering Materials and Building Preservation, School of Mechanical and Civil Engineering, Helmut Schmidt University Hamburg, Germany. Email: sylvia.kessler@hsu-hh.de.

SUPPORTING INFORMATION

Additional supporting information can be found online in the Supporting Information section at the end of this article.

How to cite this article: Nichani K, Uhlig S, Martin VS, Jaelani Y, Frost K, Beering C, et al. Time-domain analysis of signal morphology and features as suitable surrogates for structural monitoring. Structural Concrete. 2025. https://doi.org/10.1002/suco.70315

17517648, 0, Downloaded from https://onlinelibrary.wiley.com/doi/10.1002/suco.70315 by Universitätsbibliothek, Wiley Online Library on [09/09/2025]. See the Terms and Conditions (https://onlinelibrary.wiley.com/terms-and-conditions) on Wiley Online Library for rules of use; OA articles are governed by the applicable Creative Commons License